Final Report

LABORATORY TESTING OF CORE MATERIALS FROM THE RAFT RIVER GEOTHERMAL SITE

by

P. E. Peterson
R. G. Van Buskirk
F. M. Prater
C. S. Muller
J. L. Bergosh

Submitted to:

Department of Energy
Division of Geothermal Energy
Idaho Operations Office
550 Second Street
Idaho Falls, Idaho 83401

Attn: Ms. S. Prestwich

Submitted by:

Terra Tek Research
University Research Park
420 Wakara Way
Salt Lake City, Utah 84108

TR 81-75
October, 1982

ABSTRACT

Material properties of geothermal well cores were determined by testing at simulated in situ conditions. Tests were performed on core materials from the Raft River Geothermal site, Raft River, Idaho at simulated in situ geothermal conditions of overburden stress, pore fluid pressure, temperature and pore fluid chemistry. These tests provide data on physical properties, thermal conductivity, thermal diffusivity, thermal expansion, compressive strength, elastic moduli, ultrasonic velocities. Detailed technical discussions of the testing procedures are contained in the appendix where appropriate.

The testing was performed for the Department of Energy/Division of Geothermal Energy, Idaho Operations Office under Contract No. DE-AC07-77ET 28301.

TABLE OF CONTENTS

LIST OF FIGURES

List of Figures (continued)

LIST OF TABLES

INTRODUCTION

Presented here are the results of laboratory tests which were performed to determine mechanical, fluid and thermal properties of Raft River, Idaho, KGRA, geologic materials. The objective of this testing was to provide rock properties data which support calculations of geothermal reservoir capacity, life and performance. Tests were conducted on samples of competent core material taken from Raft River KGRA wells at depths of 1220 m (4000 ft) to 1520 m (5000 ft).

Tests conducted included several basic physical properties, mechanical response to stress (triaxial compression), thermal conductivity, thermal diffusivity, thermal expansion, permeability, and ultrasonic velocities. Test conditions, which simulated the geothermal environment, were 34.5 MPa (5,000 psi) overburden stress of 2.26×10^{-2} MPa/m (1 psi/ft), pore fluid pressure of 15.5 MPa (2250 psi), and temperatures of 23°C (73°F) to 150°C (300°F). Physical property tests were performed at bench conditions.

Presented in this report, in descriptive subsections specific to each type of test, are technical details and experimental results of the testing program. Each subsection provides a description of sample preparation, experimental procedure, results and conclusions. Test data are presented in summary graphs or tables in each subsection. Brief technical discussions of experimental techniques are given in the Appendix where appropriate.

Also included in this report is a geologic description of the Raft River Valley. The geologic description provides background information about the geothermal resource site and about the mineralogy of core tested in this program.

An outline of the program and a description of tests and test conditions is given in Table 1.

Table 1

Raft River

Geologic Material Characterization, Test Descriptions and Conditions

TEST DESCRIPTION	TEST CONDITIONS			
	Temp. (°C)	Confining Stress (MPa)	Pore Fluid Pressure (MPa)	Number of Samples Tested
Thin Section Analysis	N/A	N/A	N/A	8
Physical Properties				
Bulk Density (dry)	23	atmos.	atmos.	21
Bulk Density (wet)	"	"	"	"
Grain Density	"	"	"	"
Total Porosity	"	"	"	"
Saturation %	"	"	"	"
Mechanical Response				
Failure Strength	150	34.5	1.38	4
Versus Effective		34.5	15.50	4
Stress		20.7	9.52	4
		3.45	2.07	4
Failure Strength	90	34.5	15.50	4
Versus Temp.	120	34.5	15.50	4
Thermal Conductivity	30-150	34.5	15.50	4
Thermal Diffusivity	80-150	34.5	15.50	3
Thermal Expansion	30-180	34.5	15.50	4
Liquid Permeability	23-150	34.5	15.50/	4
			1.38	4
Ultrasonic Velocity	23-150	34.5	15.50	4

FACILITIES DESCRIPTION

Testing for this program was performed at Terra Tek's geothermal testing facility, Figure 1. General capabilities of this high pressure-high temperature test facility are:

- Confining pressure to 200 MPa (30,000 psi)
- Temperature to 400°C (800°F)
- Axial load to 4.5 x 10^6N (10^6 lbs)
- Sample size: 5 cm (2") diameter (to 400°C)
  10 cm (4") diameter (to 150°C)

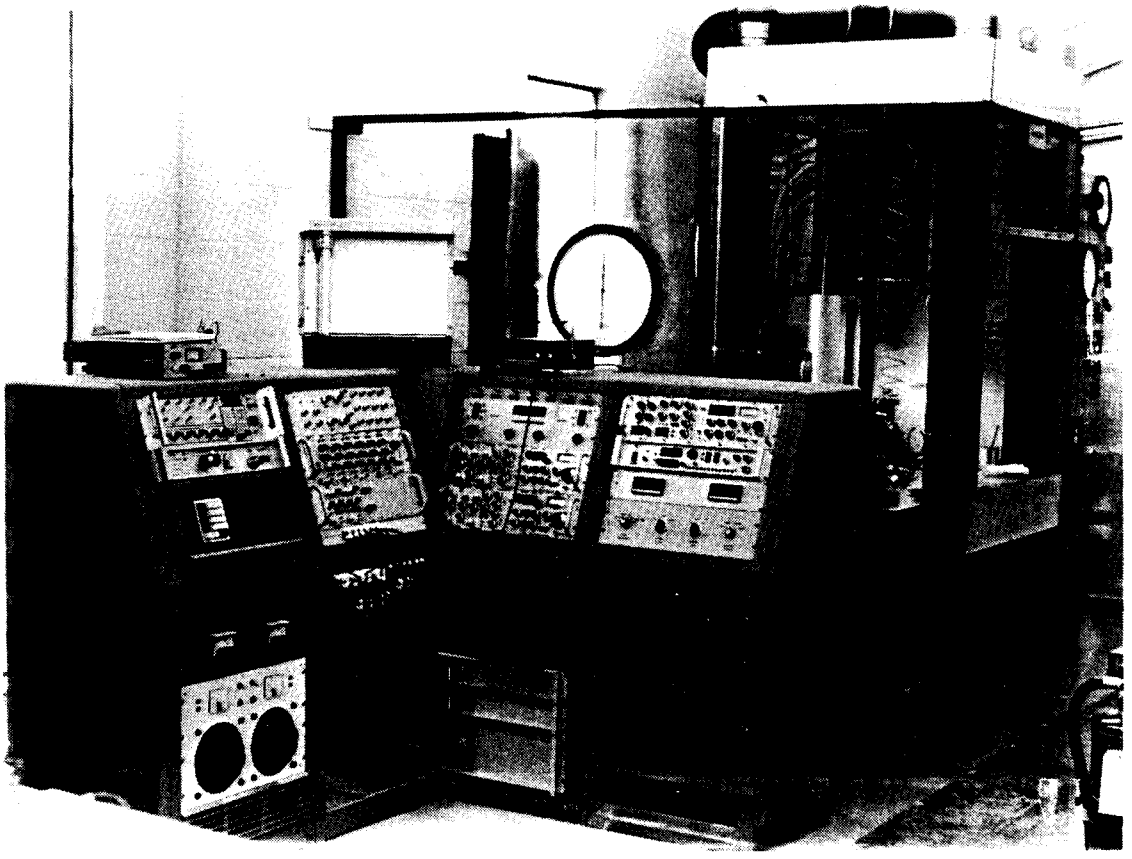

Figure 1. Geothermal Testing Facility

GEOLOGY OF THE RAFT RIVER GEOTHERMAL SITE

The Raft River Valley, a north-trending Cenozoic depression bounded on the east, south, and west by mountains, is located at the northern edge of the Basin and Range province just south of the Snake River plain (Figure 2). The geology of the valley is well defined as a result of studies by the U.S. Geological Survey (USGS)(Mabey, et al., 1978; Keys and Sullivan, 1979). The southern Raft River Valley, south of Malta, Idaho, was designated a Known Geothermal Resource Area (KGRA) in 1971 by the USGS (Godwin, et al., 1971) on the basis of two shallow wells that flow boiling water.

The Raft River Valley has subsequently been the site of many geothermal wells. The USGS has drilled 35 auger holes less than 30 m deep and 5 intermediate depth core holes up to 427 m deep. Additionally, the Idaho National Engineering Laboratory (INEL), funded by the Energy Research and Development Administration (now Department of Energy), has drilled three test wells, as deep as 1829 m, that may be used for production. Also at this site is a shallower well for reinjection of produced geothermal water.

Rocks penetrated in the INEL wells consisted of alluvium and Tertiary deposits extending to depths of approximately 1371 m. Contained in these deposits were unconsolidated to well-consolidated sandstone, siltstone, claystone, and conglomerate, some of which were tuffaceous. The deposits are underlain by Precambrian metasedimentary rocks, chiefly quartzite and schist, and quartz monzonite. The base of the Tertiary is at 1402 m in well RRGE-1*, at 1419 m in well RRGE-2*, and at 1643 m in well RRGE-3*. These points sug-

*Designations specified by INEL as Raft River Geothermal Exploratory (RRGE) well.

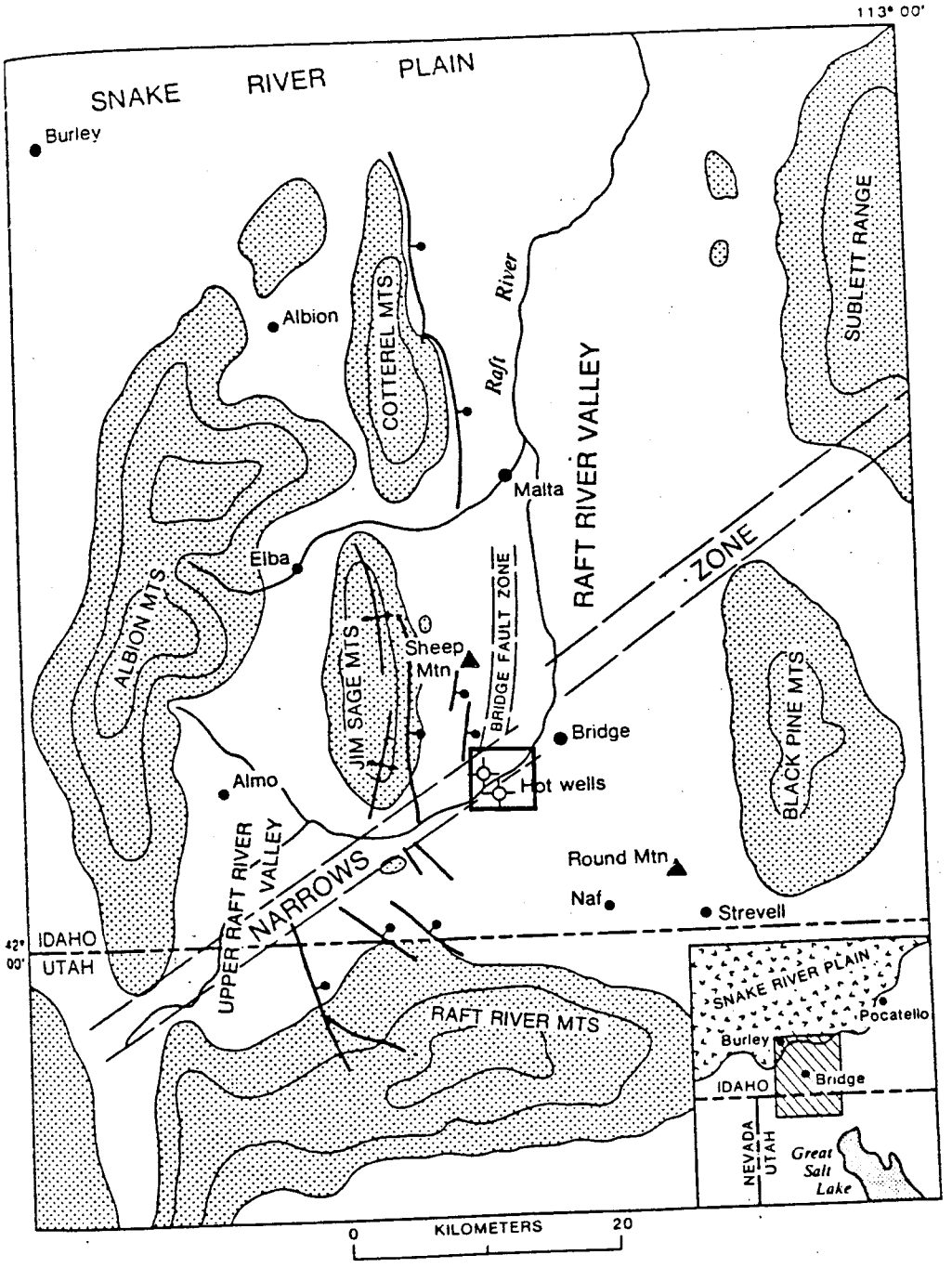

Figure 2. Map of the Raft River Valley Area (from Mabey, et al, 1978).

gest a formation dip of 7 degrees and a strike of S53°E if there are no faults between the wells.

Generally, the rocks above 1020 m are represented by a wider range of lithology and are not as well cemented as the underlying rocks. The description of the cuttings by Oriel and Williams (1975) of the USGS indicates a contact at 997 m between tuffaceous sediments above and mostly altered tuffs below. The alteration minerals were reported to include zeolites, quartz, and chalcedony which could account for the increased cementation. None of the logs provided a basis for recognizing the rhyolite and volcanic glass reported in the cuttings, however, a change to less altered rocks below 1378 m is clearly defined on the logs. Hydrothermal alteration is extensive in the deeper part of the Raft River reservoir, but data on its character are scarce. There is an interval of biotite schist, approximately 30 m in thickness, present between the Precambrian quartzite and the overlying Salt Lake formation in all three RRGE wells (Keys and Sullivan, 1979).

The Cenozoic basin fill, nearly 1,600 m of silt, sand, and gravel, accumulated by fluvial processes that have been essentially continuous for at least 7 million years. Rapid lateral changes of both facies and thickness, dips as great as 30° and alteration of the sediments make basinwide correlation of any depositional unit very difficult. Widespread observations indicate a general decrease in the gravel content and increase in hydrothermal alteration at greater depths. The entire Tertiary section contains volcanic glass shards; alteration is most evident in the types of clays derived from the glass, and in the formation of zeolites. In three of the deep boreholes studied, the clays change downward from montmorillonite to mixed-layering to illite while the zeolites change from clinoptilolite to analcite to wairakite to laumontite (Peter Kolesar, written commun., 1979). Near the base of the Cenozoic succession, deposition of silica and calcite is the dominant form of alteration.

The silica tends to form a "caprock" above the geothermal reservoir, whereas the calcite preferentially fills cracks and openings. In some places calcite and silica replace the clay and volcanic glass in the sediments.

Frequency of faults and fractures also increases with depth in the Cenozoic Basin. In the upper part of the basin fill the faults dip steeply (60°-80°) and with increasing depth, these faults decrease in dip until they become nearly horizontal at the base of the Cenozoic fill.

The basin is floored with autochthonous Precambrian and Cambrian quartzites and schists that can be correlated with formations found in the Raft River Range. These formations are the quartzite of Yost (at the top), the schist of the Upper Narrows, the Elba Quartzite, and an unnamed schist. Beneath these units is the Precambrian adamellite. These autochthonous formations, as well as the adamellite basement are generally unaltered by the geothermal fluids. They are fractured in some areas, but do not represent a significant part of the geothermal resource.

The basic model for the Raft River geothermal system has not changed significantly from that proposed by Williams and others (1976), except for the recognition of major, nearly horizontal, faults and their roles in the geothermal reservoir. The geothermal system is the result of deep circulation of meteoric water, presumably from the Albion, Goose Creek, and Raft River Mountains, along major faults. With a high regional heat flow of 2-3 microcal/cm^2sec (Urban and Diment, 1975), water need only descend to depths of 3-5 km to be heated to nearly 150°C. The heated water migrates upward along the Narrows structure, illustrated in Figure 3, to the base of the Cenozoic basin fill where it moves into the fracture-dominated reservoir.

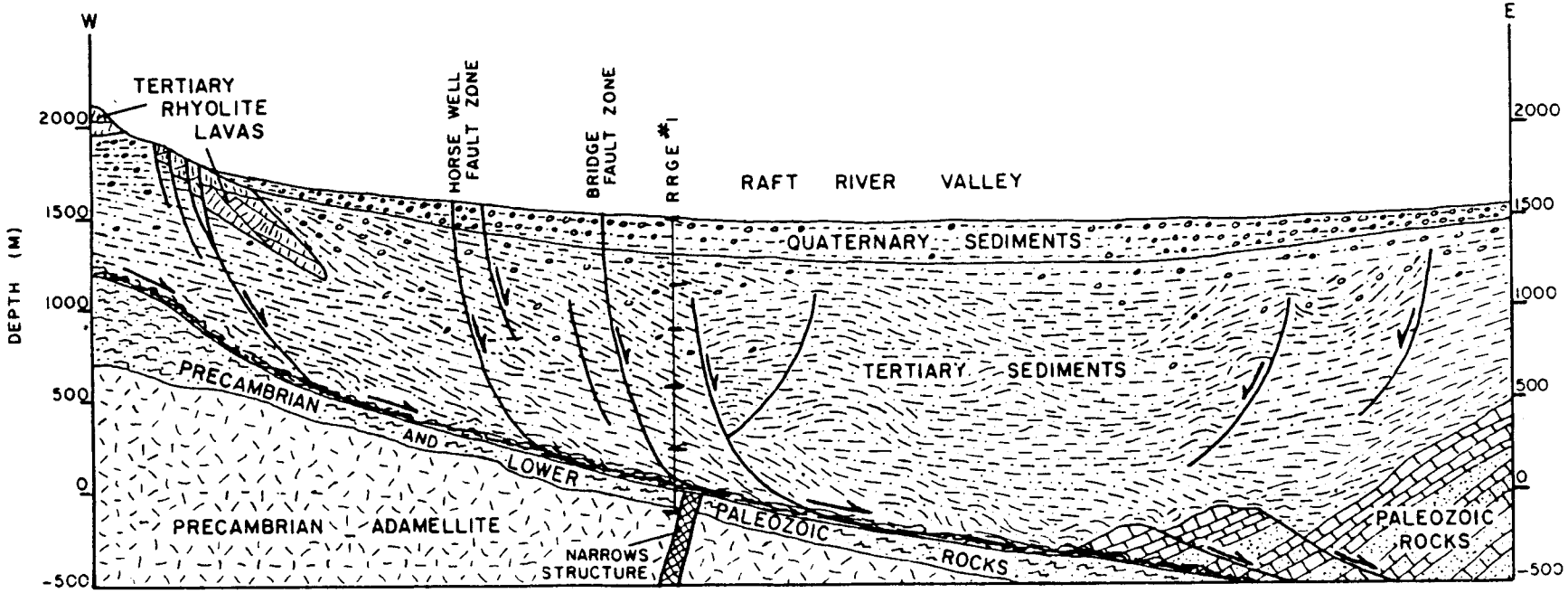

Figure 3. Generalized Cross Section of the Southern Raft River Valley, Idaho, Showing Interpretative Subsurface Geology and Structure. Arrows show direction of fault movement. Raft River Geothermal Exploration Well #1 (RRGE #1)(from Covington, 1980).

PETROGRAPHIC ANALYSIS

Samples from the four wells, RRGE #1, #2, #3C and #4B, in the Raft River area were examined in thin-section. The samples were from 1286 m, 1372 m, 1373 m, 1414 m, 1415 m, 1518 m, 1519 m, and 1519 m in the Salt Lake Formation. Clay mineralogy of two samples, from 1372 m and 1519 m, was also examined by x-ray diffraction.

Results of Analysis

Rock Types - All of the samples examined originally contained significant amounts of vitric ash. Variable amounts of silt- and sand-sized clasts occur intermixed with the vitric ash. All of the samples, except 1372 m, originated as water-lain sediments. Sample 1372 m may have originated as an airfall tuff; it contains very little silt or sand. Results of thin section analysis, performed on RRGE core samples, are presented in Table 2.

Alteration - The major effect of hydrothermal alteration has been the replacement of primary vitric ash by variable proportions of clays, calcite and very fine-grained quartz and feldspar. Detrital biotite grains have been in part replaced by chlorite. Feldspars have been locally partially replaced by zeolites and illite. Very fine-grained pyrite occurs as disseminations; whether it is primary or secondary is not obvious. Fractures have been lined by zeolites; their centers have been partially or completely filled by calcite.

X-ray diffraction analyses indicate that kaolinite (7A) and illite (10A) occur in sample 1372 m. Sample 1512 m contains a clay at 28A (possibly mixed layer chlorite-smectite) and illite (10A). XRD peaks of the zeolite in veins at 1372 m suggest that it is a member of the harmotome group.

Table 2

Thin Section Analysis of Salt Lake Formation Samples
(4200 ft to 5000 ft)

Sample Depth (m)		1286	1372	1373	1414	1415	1518	1519	1519
Well*:		RRGE #2	RRGE #1	RRGE #1	RRGE #4B	RRGE #4B	RRGE #3C	RRGE #3C	RRGE #3C
Rock Name:		Graywacke	Devitrified Tuff	Silty Mudstone	Silty Devitrified Tuff	Silty Devitrified Tuff	Silty Tuff & Graywacke	Silty Devitrified Tuff	Silty Devitrified Tuff
PERCENT CONSTITUENTS	Quartz	25	38	18	10	26	39	10	20
	Orthoclase/ Microcline	25	19	20	7	23	24	25	15
	Plagioclase	25	--	18	7	14	5	15	6
	Sericite/ Muscovite	5	--	10	8	8	2	2	2
	Chlorite/ Biotite	10	3	3	2	2	2	6	--
	Zeolites	4	3	--	--	1	2	1	1
	Calcite	6	2	10	6	8	9	--	6
	Albite	--	28	--	--	--	--	--	--
	Kaolinite	--	5	--	--	--	--	--	--
	Illite	--	2	--	--	--	--	--	--
	Pyrite	--	--	1	--	--	--	1	--
	Clay	--	--	20	60	18	17	40	50

*INEL Designation

The rocks in the 1286 m to 1519 m interval have been subjected to low temperature, low to moderate salinity fluids. These rocks have been fractured since deposition, but alteration products have closed the fractures and current permeability and porosity are low.

PHYSICAL PROPERTIES TESTS

Several physical properties of core from the four Raft River wells were measured to provide basic rock characterization. Properties measured include: dry bulk density, wet (as-received) bulk density, grain density, total porosity, and as-received percent saturation. Twenty-one samples, from depths of 1286 m (4219 ft) to 1519 m (4983 ft), were tested. Samples were taken from wells RRGE #1, #2, #3C and #4B.

Test Procedures

Sample Preparation

Samples, greater than 100 cc, were broken from the original core, wrapped in aluminum foil and waxed to preserve moisture content until testing began.

Experimental Procedure

Bulk Density: The bulk density was determined by weighing the test specimen and measuring its volume using the mercury displacement technique. The specimen was then oven dried and weighed. The original weight divided by the volume yields the bulk density, and the dried weight divided by the volume yields the dry density.

$$\text{Bulk Density: } W\ DEN = \frac{\text{orig. wt.}}{\text{vol.}} \qquad \text{Dry Density} = D\ DEN = \frac{\text{dry wt.}}{\text{vol.}}$$

Grain Density: The specimen was crushed and pulverized to 100 mesh particles. Grain volume was measured by water immersion and gas evacuation techniques. Weights are accurate to 0.1 percent and volumes are accurate to 1.0 percent. Grain density was found by dividing grain weight by grain volume

$$\text{Grain Density: } G\ DEN = \frac{\text{grain wt.}}{\text{grain vol.}}$$

As-Received Water Content: The water in the as-received specimen was found by subtracting the specimen's dry weight from the as-received weight and dividing the resultant by the as-received weight.

$$\text{As-Received Water Content: } \%\ W = \frac{\text{orig. wt. - dry wt.}}{\text{orig. wt.}}$$

Total Porosity: The specimen porosity or void volume was derived from the dry density and the grain density as follows:

$$\text{Total Porosity: } POR\% = 1 - \frac{D\ DEN}{G\ DEN} \times 100\%$$

Physical Properties Test Results

Results of the physical properties determinations are given in Table 3. A total of 21 samples from the four Raft River wells were tested. Six types of rock are represented in these samples, which were taken from the Salt Lake Formation.

Discussion and Conclusions

Bulk densities ranged from 1.95 g/cc to 2.42 g/cc and grain densities ranged from 2.70 g/cc to 2.91 g/cc. Density values for each type of rock are somewhat variable and no strong trend of density as a function of depth of burial is evident.

Only trace amounts of water were found in the core and subsequently the as-received saturation of the rocks did not exceed 10%. This result was probably obtained because no attempt was made during the coring and subsequent storage to preserve the natural water content of the samples.

Porosity ranged from 14.6% to 30.4%. Porosity values varied substantially within groups of samples from a given depth, and no trend in porosity with depth of burial is evident.

The large variation in the physical properties data reflect the high degree of variability seen in the samples extracted from the Salt Lake formation.

Table 3

Physical Properties of Raft River KGRA Core Samples

Well*	Sample Depth (m)	Rock Description	Density (gm/cc)			% Porosity	S_{water} (%)
			Wet	Dry	Grain		
RRGE #2	1286	Graywacke	2.06	2.05	2.90	29.1	2.8
RRGE #2	1286		2.39	2.38	2.82	15.5	6.4
RRGE #2	1288		2.27	2.26	2.81	19.5	4.6
RRGE #2	1288		2.26	2.25	2.70	16.5	3.6
RRGE #1	1372	Devitrified Tuff	1.95	1.94	2.79	30.4	1.0
RRGE #1	1373	Silty Mudstone	2.03	2.02	2.70	25.1	1.4
RRGE #1	1373		2.13	2.12	2.82	24.7	3.6
RRGE #1	1373		2.35	2.34	2.75	14.9	8.4
RRGE #1	1374		2.34	2.33	2.80	16.9	7.2
RRGE #4B	1414	Silty Devitrified Tuff	2.35	2.34	2.75	14.6	4.2
RRGE #4B	1414		2.20	2.19	2.83	22.6	4.5
RRGE #4B	1414		2.28	2.26	2.78	18.6	6.1
RRGE #4B	1415		2.32	2.31	2.88	19.9	3.7
RRGE #4B	1415		2.29	2.27	2.88	21.1	5.9
RRGE #4B	1416	Silty Devitrified Tuff	2.29	2.28	2.82	19.1	4.3
RRGE #4B	1416		2.27	2.26	2.75	17.9	3.7
RRGE #3C	1519	Silty Tuff & Graywacke	2.41	2.40	2.87	16.6	9.5
RRGE #3C	1519		2.42	2.41	2.91	17.0	3.4
RRGE #3C	1519		2.17	2.15	2.76	22.2	8.0
RRGE #3C	1519	Sandy Devitrified Tuff	2.24	2.22	2.81	21.0	9.9
RRGE #3C	1519		2.26	2.24	2.80	20.0	9.9

*INEL Designation

MECHANICAL RESPONSE TESTS (TRIAXIAL COMPRESSION)

Triaxial compression tests were performed on cores from the four Raft River wells to define material failure envelopes, and to determine the effect of temperature on material failure strength. To generate these data, six samples from each well were tested.

Triaxial failure envelopes were defined by testing four samples at a different effective stress (1.4 MPa, 11.2 MPa, 19.0 MPa and 33.1 MPa) while test temperature was maintained at 150°C.

Effect of temperature upon material strength was determined by testing two additional specimens at different temperatures (90° and 120°C) while maintaining an effective stress of 19 MPa.

Test Procedures

Core materials for testing were prepared as right circular cylinders, 5.08 cm (2.00 inches) in length and 2.59 cm (1.00 inch) in diameter. Sample ends were ground flat and parallel to ±0.013 m (±0.005 inches). Hardened steel endcaps were placed at each end and the assembly was jacketed with teflon tubing to isolate the sample from the confining fluid. Strain measuring devices were positioned on the endcaps to record axial strains, and a lateral strain measuring device was placed on the sample diameter at the mid-point of the sample length. Prepared samples were placed in a triaxial test machine, saturated with synthetic brine by vacuuming and flooding, and allowed to come to equilibrium with temperature and pore fluid pressure. Generally, pore pressure reached a constant equilibrium value throughout the sample after a period of 2 hours at *in situ* conditions. Equilibrium was assumed to exist after pore fluid pressure became invarient with time. During the test, drained conditions were maintained in the sample by connecting the

pore pressure system to an external volume maintained at the desired reservoir pressure. Loading was initiated and continued to sample failure at a strain rate of approximately 10^{-4} sec^{-1}. Axial strain, lateral strain and axial stress difference were recorded continuously during loading until sample failure occurred.

Failure strength was found from the peak value of the axial stress measurement. Elastic parameters were evaluated at fifty percent of failure strength, and were calculated using the following relationships:

Elastic Modulus (Young's)

$$E = \frac{\text{axial stress}}{\text{axial strain}}$$

$$E = \frac{\sigma}{\varepsilon}$$

Poisson's Ratio

$$\nu = \frac{\text{lateral strain}}{\text{axial strain}}$$

$$\nu = \frac{-\varepsilon_x}{\varepsilon_y}$$

Shear Modulus

$$G = \frac{E}{2(1+\nu)}$$

Mechanical Response Test Results

Results of the mechanical response tests are presented in Table 4 and in Figures 4 through 9. Summary plots of triaxial failure envelopes and failure stress as a function of temperature are contained in Figures 4 and 5, respectively. Stress-strain plots for each individual well are contained in Figures 6 through 9.

Table 4

Summary of Triaxial Compression Test Results

Well	Depth (m)	Rock Description	Effective (Compressive) Stress (MPa)	Test Temp. (°C)	Elastic Modulus (MPa)	Poisson's Ratio	Shear Modulus (MPa)	Maximum $\sigma_1 - \sigma_3$ (MPa)	ε_A % at Failure
RRGE #2	1288	Graywacke	19.0	90	1,600	0.18	700	4.3	0.94
			19.0	120	10,100	0.21	4,200	42.2	1.32
			19.0	150	9,200	0.35	3,400	45.5	0.92
			33.1	150	3,200	0.10	1,500	30.3	1.21
			11.2	150	8,400	0.14	3,700	45.5	2.01
			1.4	150	1,900	0.10	900	11.6	0.60
RRGE #1	1373	Silty · Mudstone	19.0	90	11,500	0.21	4,700	36.1	1.04
			19.0	120	15,600	0.18	6,600	58.9	1.13
			19.0	150	9,500	0.13	4,200	39.5	0.64
			33.1	150	11,400	0.37	4,200	41.4	0.99
			11.2	150	7,400	0.13	3,300	59.9	1.25
			1.4	150	4,500	0.16	2,000	23.4	0.57
RRGE #4B	1414	Silty Devitrified Tuff	19.0	90	19,900	0.18	8,400	85.0	0.44
			19.0	120	34,500	0.37	12,600	93.3	1.28
			19.0	150	19,300	0.20	8,000	87.6	0.69
			33.1	150	10,200	0.08	4,700	37.4	0.11
			11.2	150	6,100	0.05	2,900	24.1	0.52
			1.4	150	5,900	0.08	2,700	30.2	0.54
RRGE #3C	1519	Silty Tuff and Graywacke	19.0	90	34,500	0.28	13,500	165.7	0.93
			19.0	120	33,700	0.29	13,100	144.1	0.60
			19.0	150	33,400	0.27	13,100	185.2	0.77
			33.1	150	46,700	0.29	18,100	190.2	0.78
			11.2	150	11,800	0.07	5,500	152.3	1.44
			1.4	150	20,500	0.11	9,200	93.7	0.43

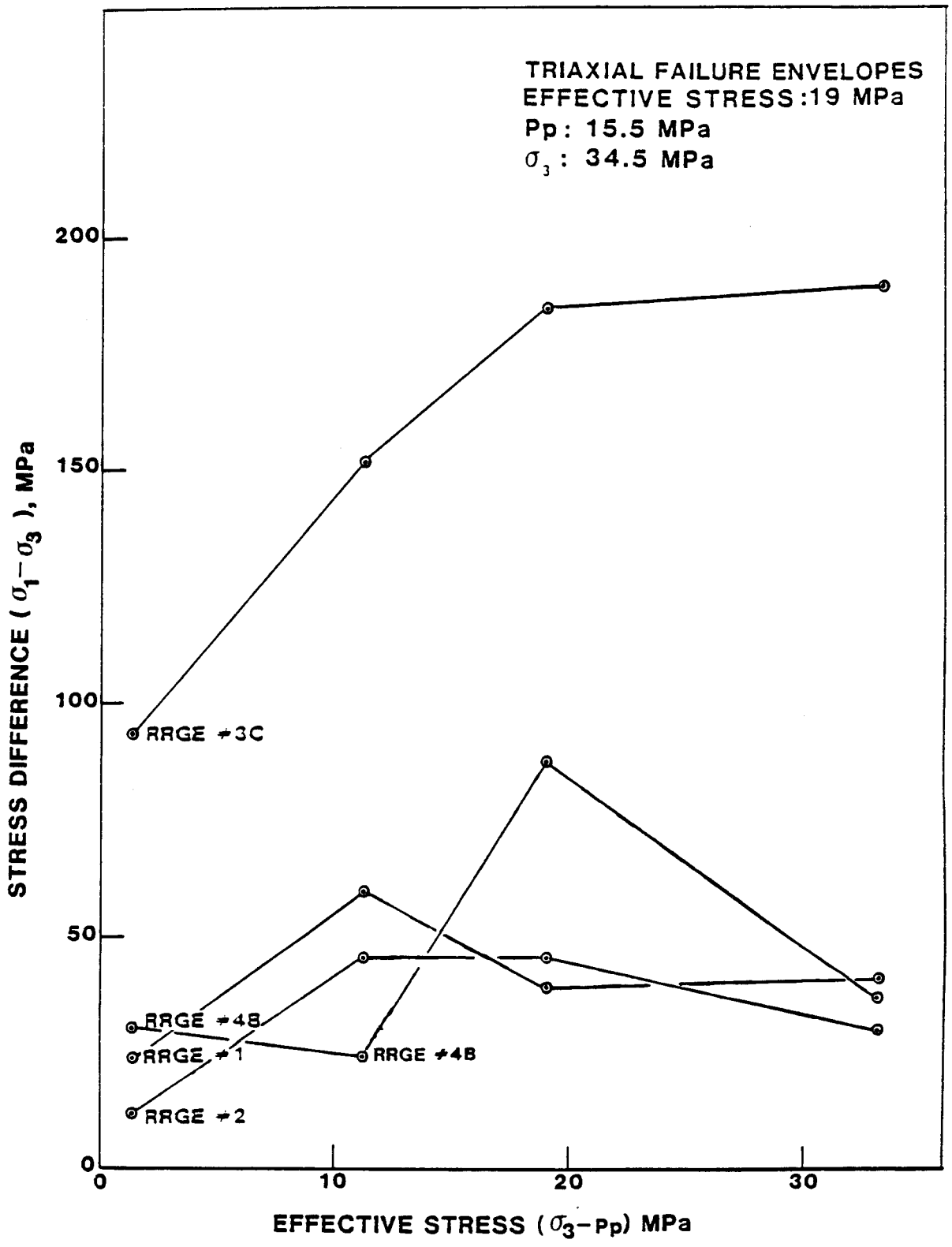

Figure 4. Summary of Triaxial Failure Envelopes for Raft River Core.

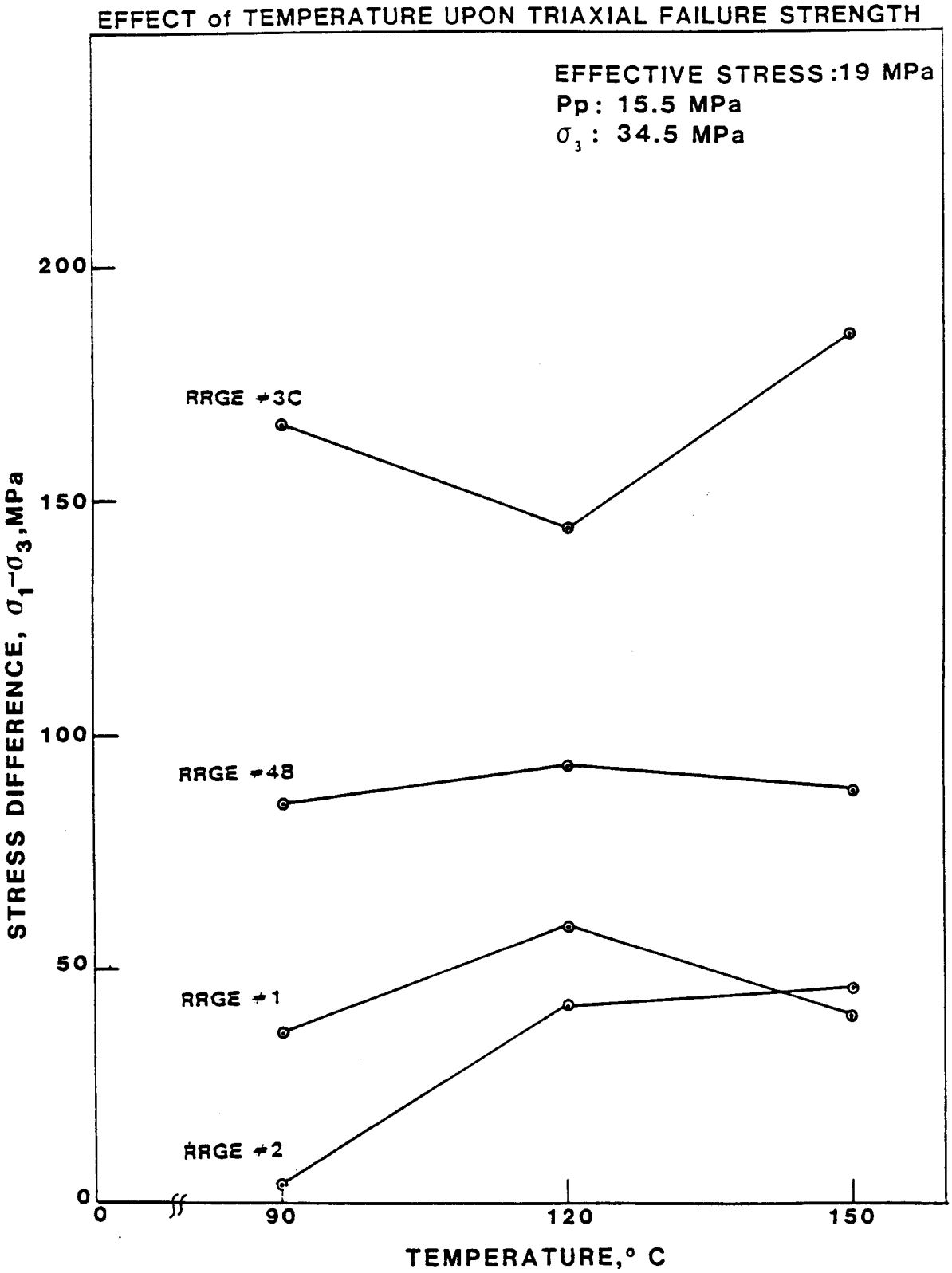

Figure 5 : Effect of Temperature Upon Triaxial Failure Strength of Raft River Core.

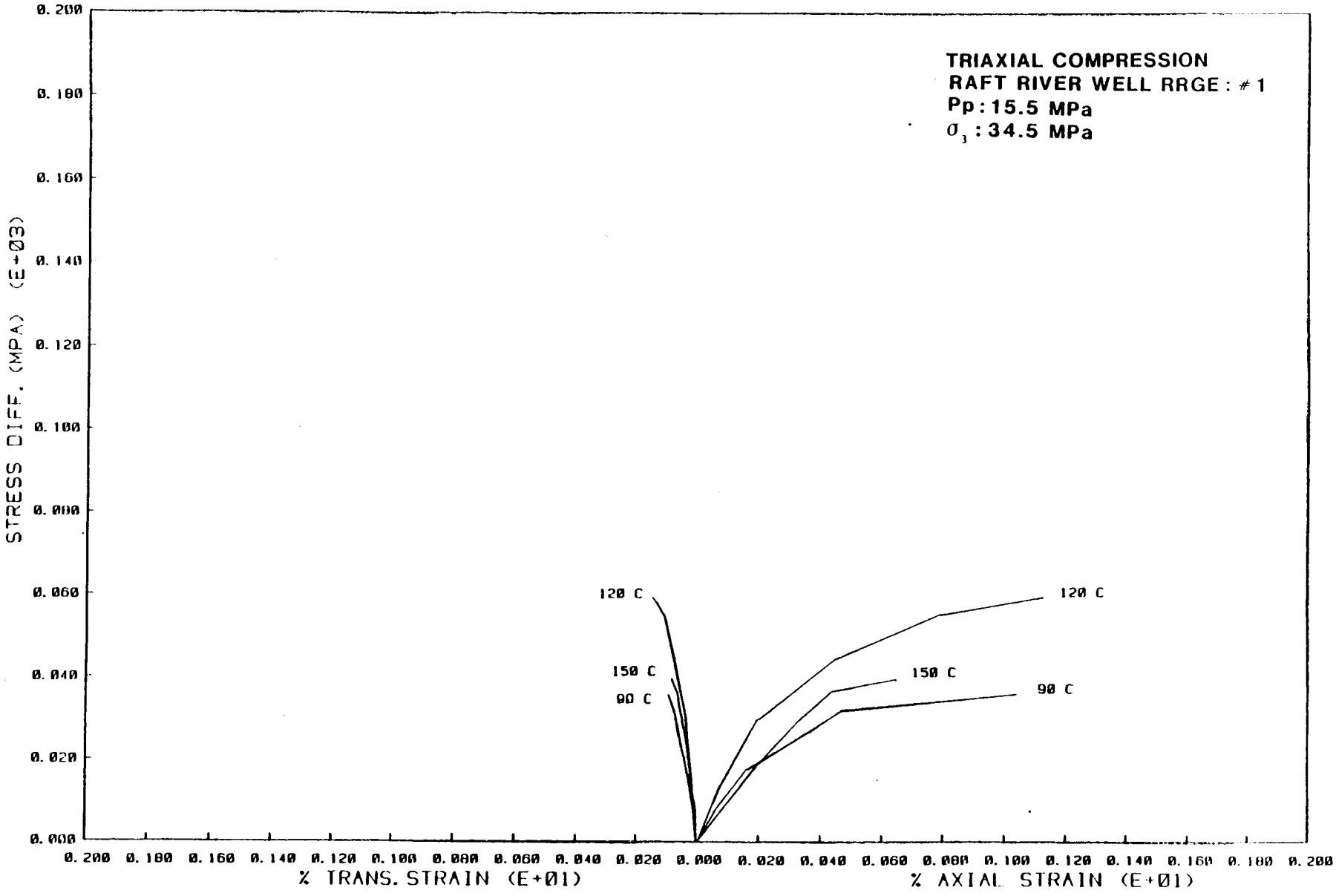

Figure 6: Triaxial Test Results for RRGE #1

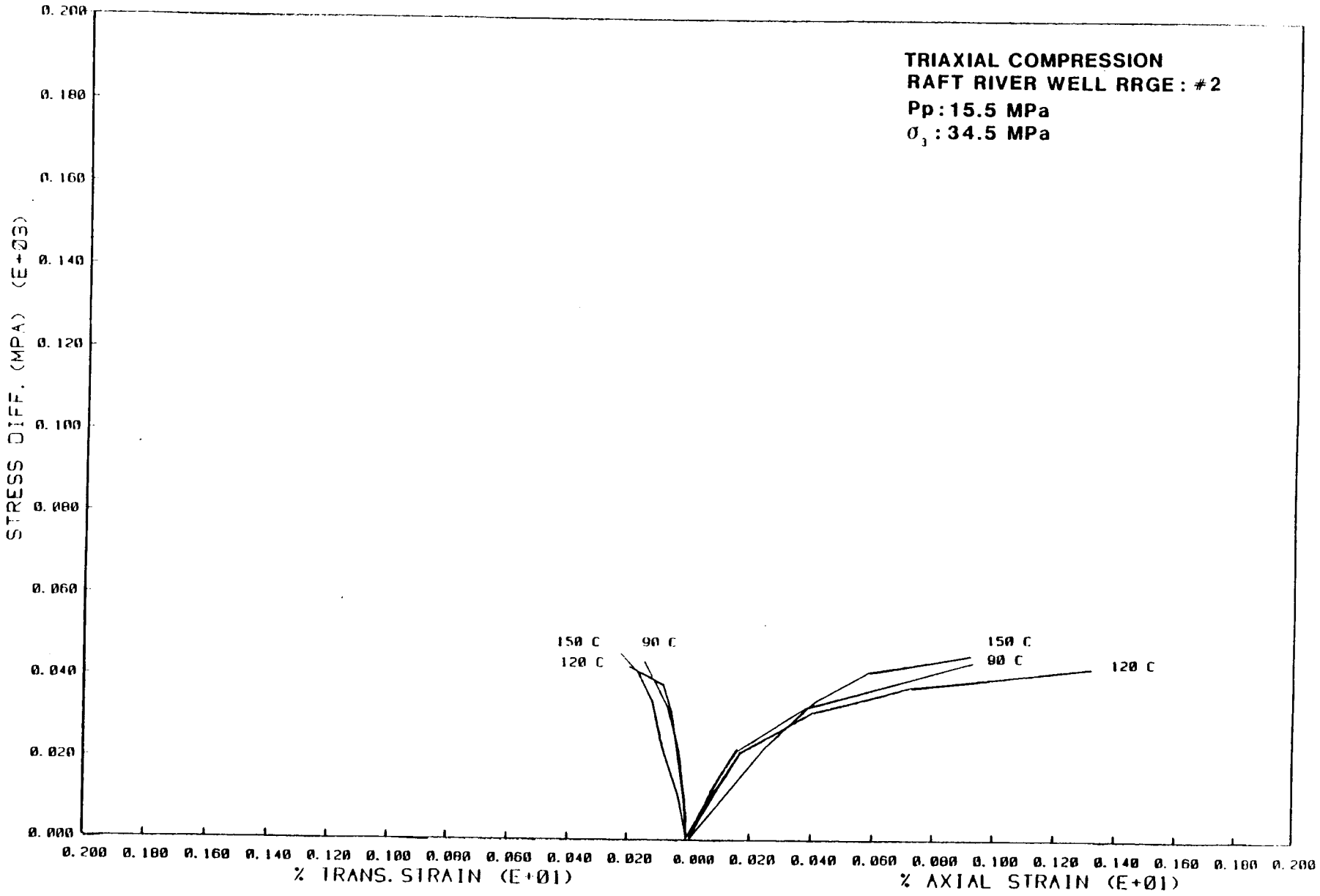

Figure 7: Triaxial Test Results for RRGE #2

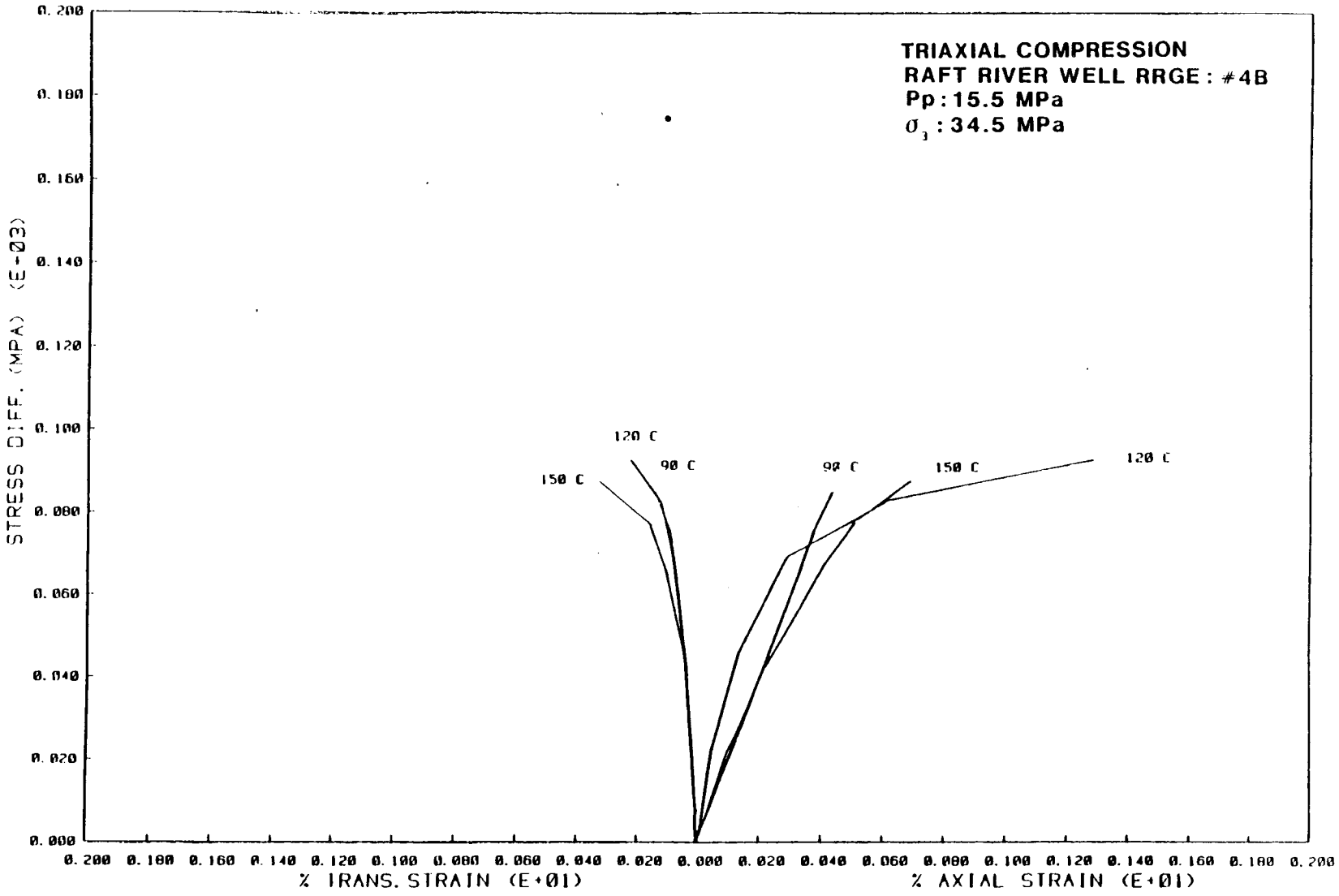

Figure 8: Triaxial Test Results for RRGE #4

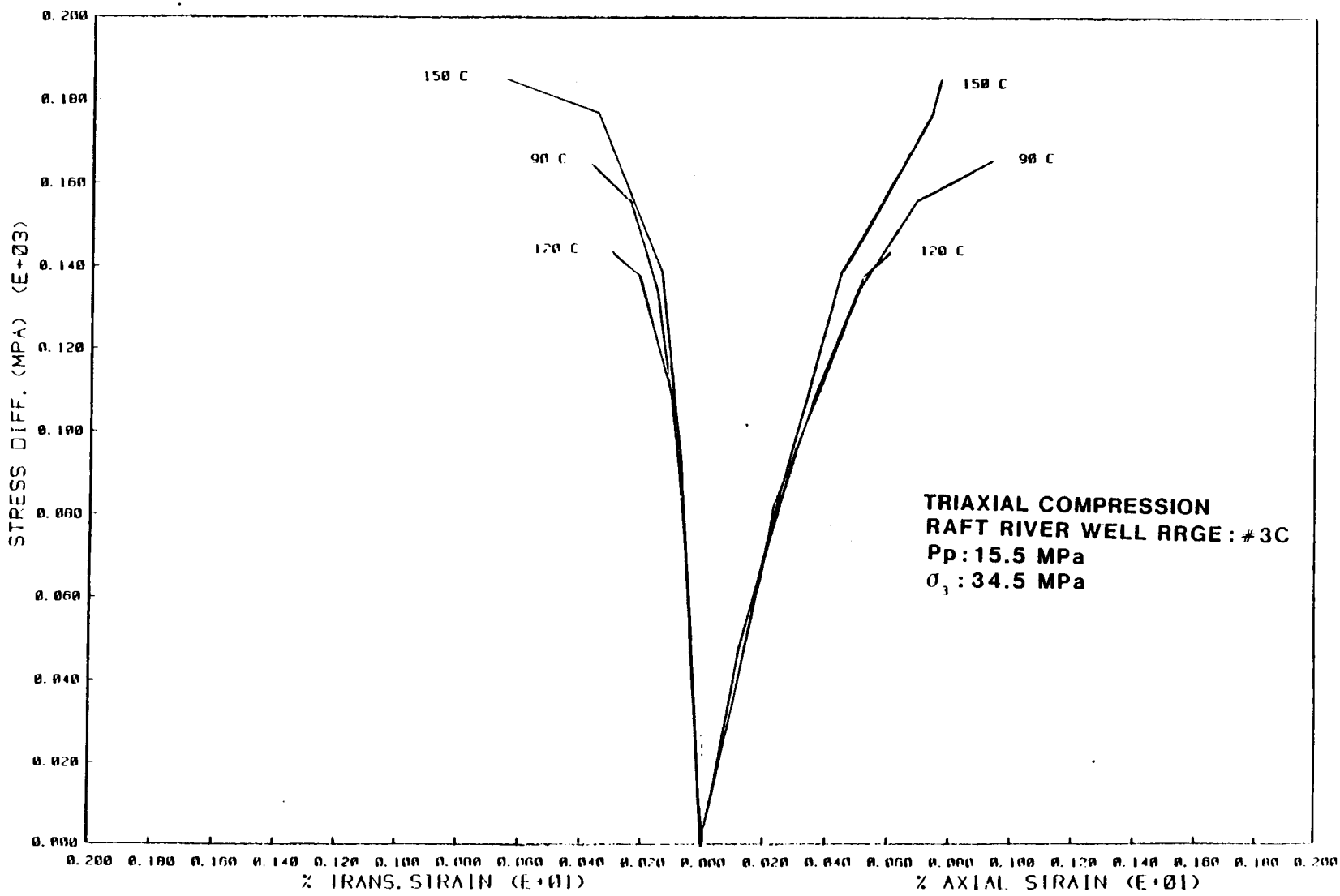

Figure 9 : Triaxial Test Results for RRGE #3

Discussion and Conclusions

As shown in Table 4, triaxial compressive strength (defined as $\sigma_1 - \sigma_3$ or axial stress minus confining stress) of the Raft River materials varied from 4.3 MPa to 190.2 MPa for the stated test conditions. The elastic (Young's) modulus of these materials varied from 1,600 MPa to 46,700 MPa and Poisson's ratio ranged from 0.05 to 0.37. Both elastic modulus and failure strength increased with increasing depth of burial; data are somewhat scattered, but these trends are evident. Poisson's ratio shows no obvious trend with depth of burial or with change in test temperature.

Triaxial failure envelopes, given in Figure 4, show that failure strength tends to increase with increasing effective stress (confining stress minus pore fluid pressure, $\sigma_3 - P_p$) until effective stress exceeds the in situ value of 19 MPa. With effective stress values greater than 19 MPa, failure strength tends to decrease. The nature of this effect is difficult to resolve given the variable nature of geologic materials and the small number of tests conducted.

Shown in Figure 5 is a weak trend for increasing strength with increasing temperature. A trend in this direction is very unusual. However, scatter in the data is relatively large, and statistical significance of this correlation is rather low. A much larger number of tests would need to be conducted to provide a reasonable data population upon which to base definitive observations.

Stress-strain response of the Raft River materials, plotted in Figures 6 through 9, shows a strong correlation with sample depth. The stress-strain plots clearly show the increased load carrying capacity with increasing sample depth. This mechanical response is, by definition, reflected in the modulus values reported in Table 4.

THERMAL CONDUCTIVITY/THERMAL DIFFUSIVITY

Thermal conductivity of one sample from each of the four Raft River wells, RRGE #1, #2, #3C and #4B, was measured as a function of temperature. Conductivity determinations were performed at in situ stress and pore fluid pressure levels and at temperatures ranging from 25°C to 150°C.

Thermal diffusivity was measured for three samples from wells RRGE #1, #3C and #4B, as a function of temperature. Diffusivity determinations were performed at simulated in situ pressure at temperatures ranging from 80°C to 150°C.

Test Procedures

Sample Preparation - Conductivity and Diffusivity

Core materials for testing were prepared as right circular cylinders, 10.2 cm (4.0 inches) in length and 5.08 cm (2.0 inches) in diameter with a 0.48 cm (0.188 inch) diameter hole along the central axis. Sample ends were cut parallel to ±0.025 cm (±0.010 inches). A line source heater and a thermocouple were inserted in the central hole through the sample, and cemented in place using a compound with high thermal conductivity. A second thermocouple was attached to the outer boundary of the sample. Steel endcaps were placed at each end of the sample and the assembly was jacketed with teflon tubing to isolate the sample from the confining fluid. Prepared samples were placed in a pressure vessel, saturated with synthetic ground water by vacuuming and flooding, and allowed to come to equilibrium with pressure and temperature. Generally, pore pressure reached a constant equilibrium value throughout the sample after a period of three hours at in situ conditions. Equilibrium was assumed to exist after pore fluid pressure became invarient with time. During the test, pressures and average temperatures were maintained at the desired reservoir conditions.

Experimental Procedure - Conductivity

Thermal conductivity values at pressure and temperature were determined using the transient line heat source ("needle-probe") method developed by Woodside and Messmer. A more complete discussion of this technique is presented in the appendix.

The samples were brought to the desired in situ pressure and temperature, then constant power was applied to the probe heater for a short period, generally less than 60 seconds. Because power is input for a short length of time, the exterior temperature of the sample does not increase. With this boundary condition, the monitoring needle probe temperature changes as though the sample were infinitely large. Since the rate of temperature rise of the probe heater at constant power is governed by the test sample properties, thermal conductivity can be calculated from the power input and the temperature history of the internal heater.

Experimental Procedure-Diffusivity

Thermal diffusivity values at pressure and temperature were determined by introducing a sinusoidal temperature oscillation at the surface of a finite cylindrical sample while the internal temperature was monitored. Under such conditions the center temperature will lag the surface temperature by some time, t_1. This measured time lag, period of oscillation, and sample radius were then used to analytically determine diffusivity as shown by Carslaw and Jaeger (1959).

The sample was convectively heated through temperature oscillations induced with heaters driven by a programmable temperature controller. The accuracy to which temperature, sample radius, period of oscillation and time lag could be determined allowed diffusivity measurements that were accurate to within ±5 percent. Tests were conducted at 34.5 MPa (5000 psi) confining

pressure and 15.5 MPa (2250 psi) pore fluid pressures at temperatures between 25°C and 150°C. Thermal conductivity determinations were performed two or more times at each stated temperature and the average of measured values is given in the results.

Thermal Conductivity/Diffusivity Test Results

Table 5 gives a compilation of thermal conductivity and thermal diffusivity test results. Figures 10 through 14 show plots of data from thermal conductivity tests conducted at in situ conditions on core samples from four Raft River wells, RRGE #1, #2, #3C and #4B. Figure 10 is a summary of the thermal conductivity test results for core from each of the four wells.

Thermal diffusivity measurements were made on three of the samples used in the conductivity testing, samples from wells RRGE #1, #3C and #4B. Pore fluid and confining pressures were maintained at the in situ values specified above. Figure 15 shows a compilation of the results of these tests.

Discussion and Conclusions

Thermal conductivity of Raft River geologic materials decreases with increasing temperature. This decrease is shown in Figure 10 where data for temperatures of 25° to 150°C are plotted. Thermal conductivity values range from 2.1 to 2.5 W/mK at 25°C and from 2.0 to 23 W/mK at 150°C. Typically, thermal conductivity decreases by 3 to 10 percent over the 25° to 150°C temperature range. The most pronounced change in conductivity occurs between 25° and 90°C, only small changes occur between 90° and 150°C.

Thermal diffusivity, which is essentially the ratio of a material's thermal conductivity to heat capacity, of the Raft River core decreases with increasing temperature. A decrease of 20 to 40 percent was measured over the temperature range of 80 to 150°C. Values of thermal diffusivity ranged from 2×10^{-3} to 7×10^{-3} cm^2/sec.

Table 5

Summary of Thermal Conductivity and
Thermal Diffusivity Test Results

Well No.*	Sample Depth (m)	Rock Type	Test Temperature (°C)	Thermal Conductivity (W/mK)	Thermal Diffusivity (cm^2/sec)
RRGE #2	1286	Graywacke	26	2.39	---
			89	2.21	---
			105	2.20	---
			150	2.19	---
RRGE #1	1372	Devitrified Tuff	22	2.05	---
			98	1.98	---
			155	1.99	1.90×10^{-3}
RRGE #4B	1415	Silty Devitrified Tuff	26	2.45	---
			85	2.27	6.80×10^{-3}
			125	2.24	3.90×10^{-3}
RRGE #3C	1519	Sandy Devitrified Tuff	26	2.37	---
			85	2.29	6.20×10^{-3}
			140	2.30	5.60×10^{-3}

*INEL Designation

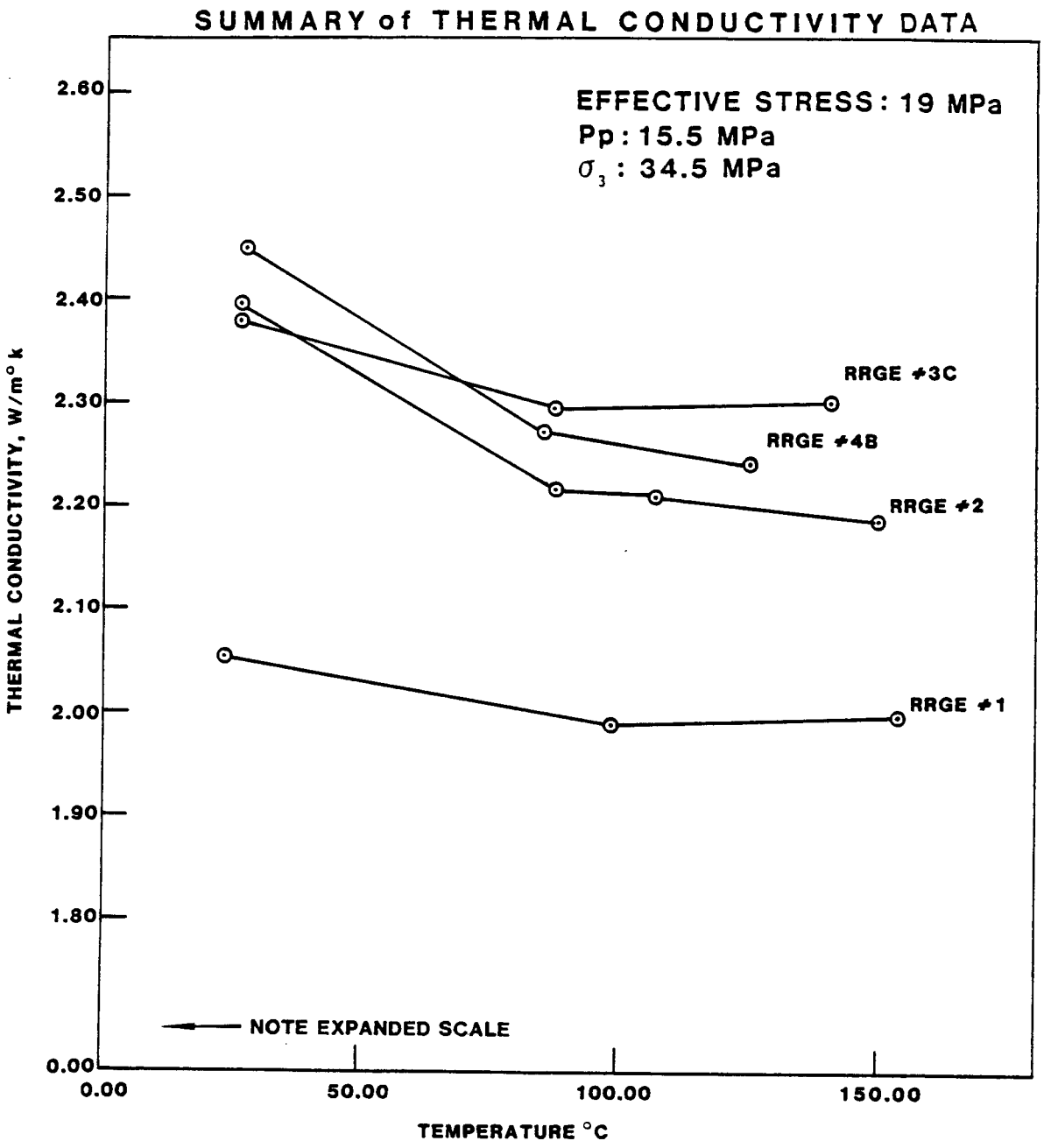

Figure 10: Summary of Thermal Conductivity Test Results.

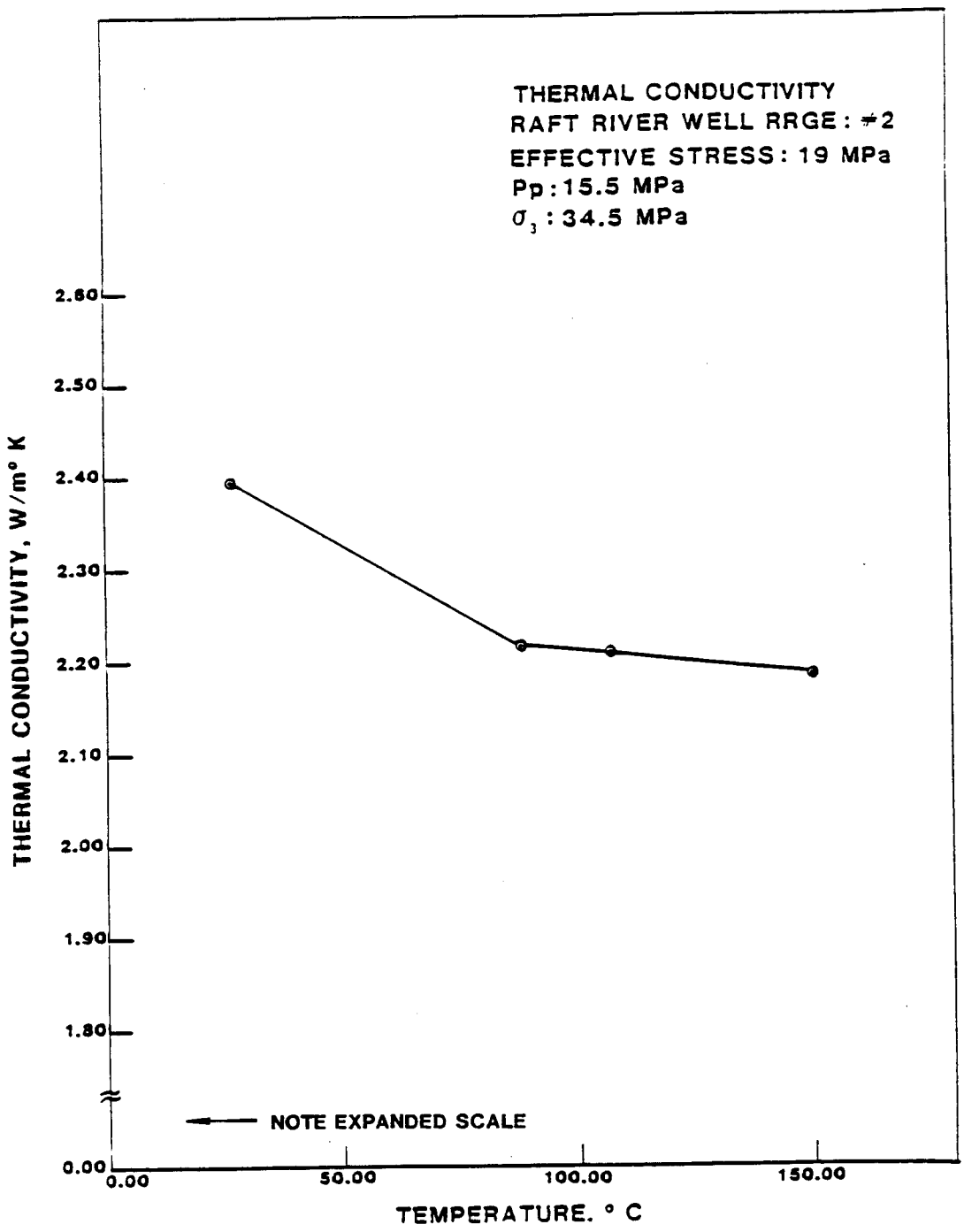

Figure 11: Thermal Conductivity vs. Temperature. Raft River Well #2.

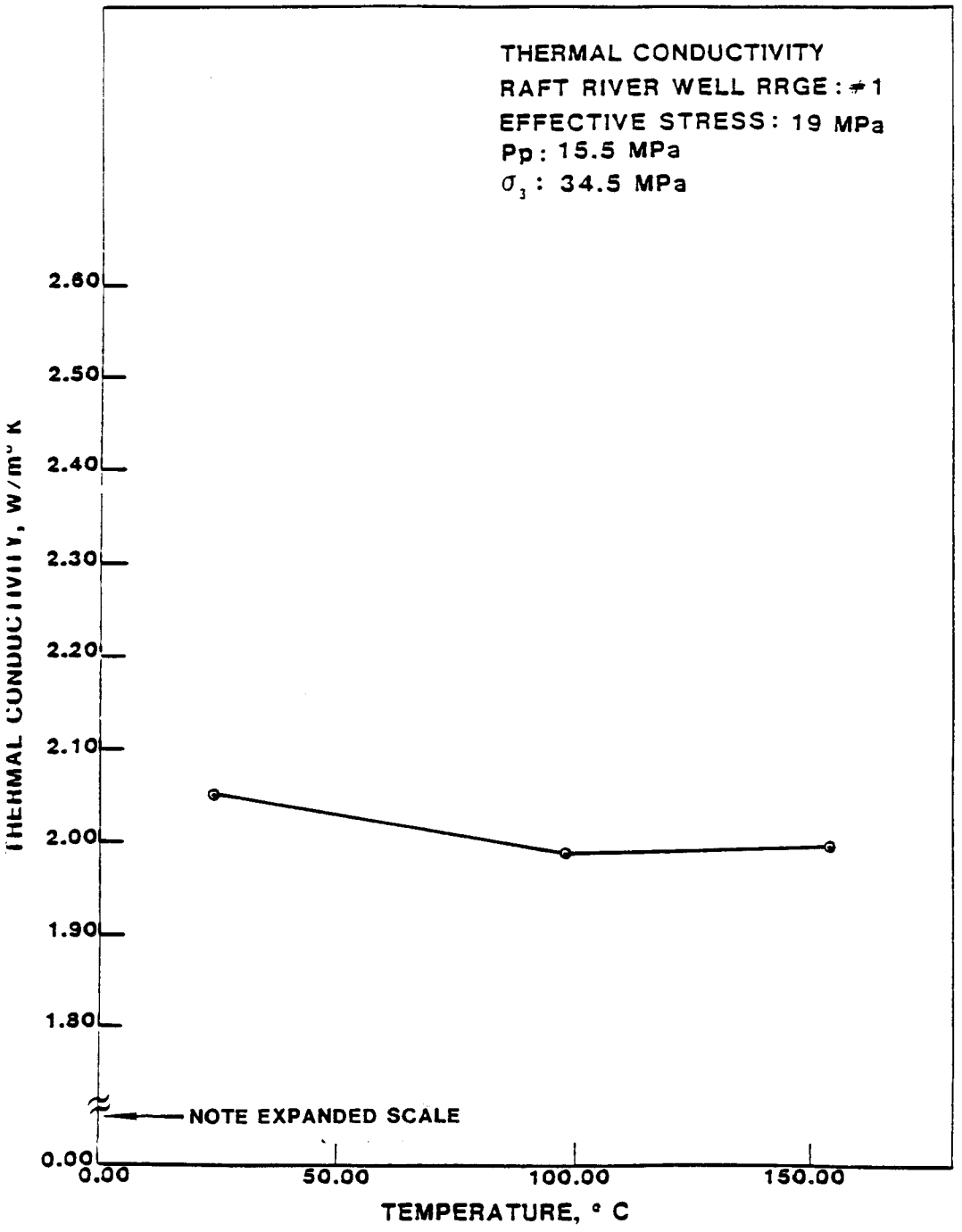

Figure 12 : Thermal Conductivity vs. Temperature. Raft River Well #1.

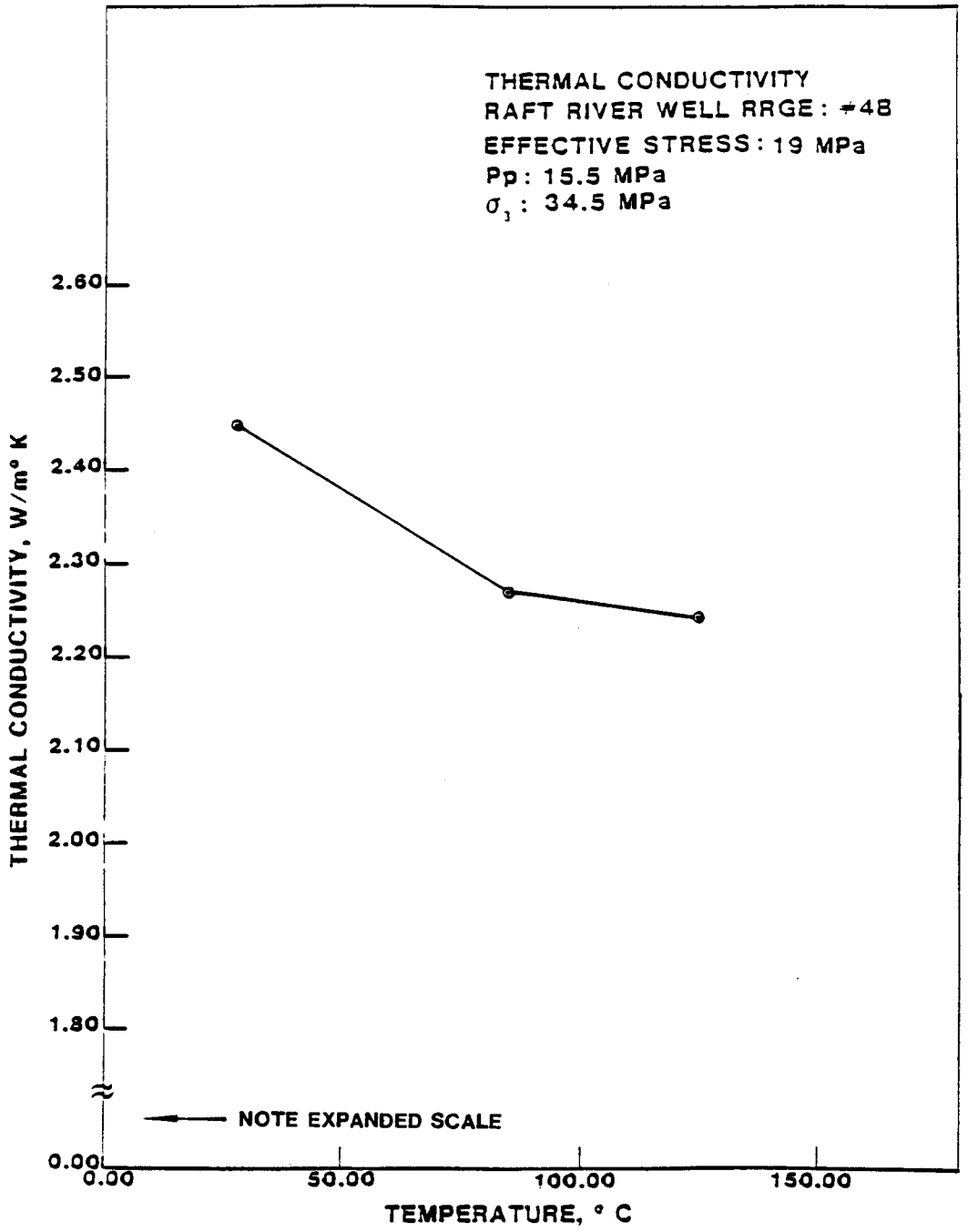

Figure 13: Thermal Conductivity vs. Temperature. Raft River Well #4B.

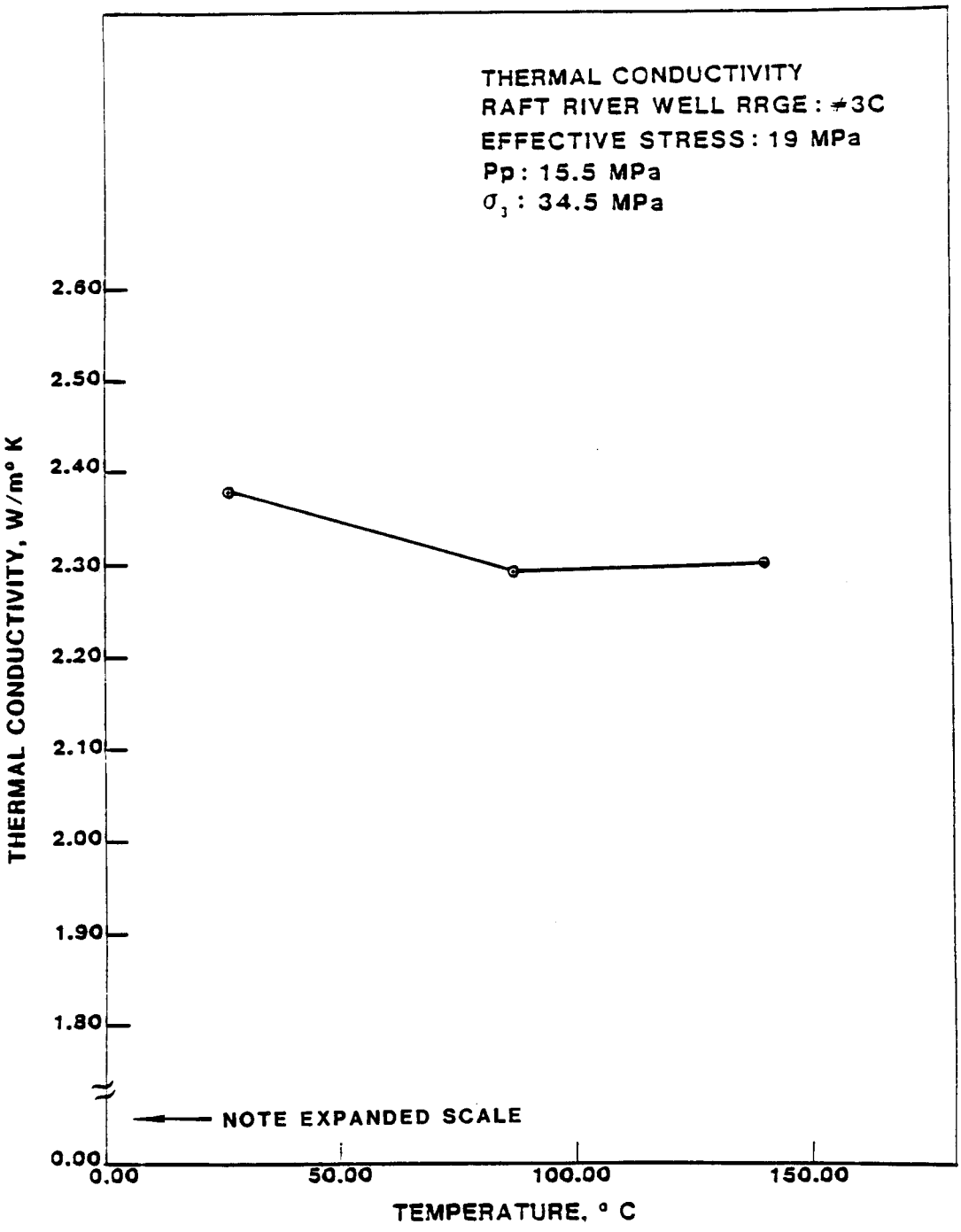

Figure 14: Thermal Conductivity vs. Temperature. Raft River Well #3C.

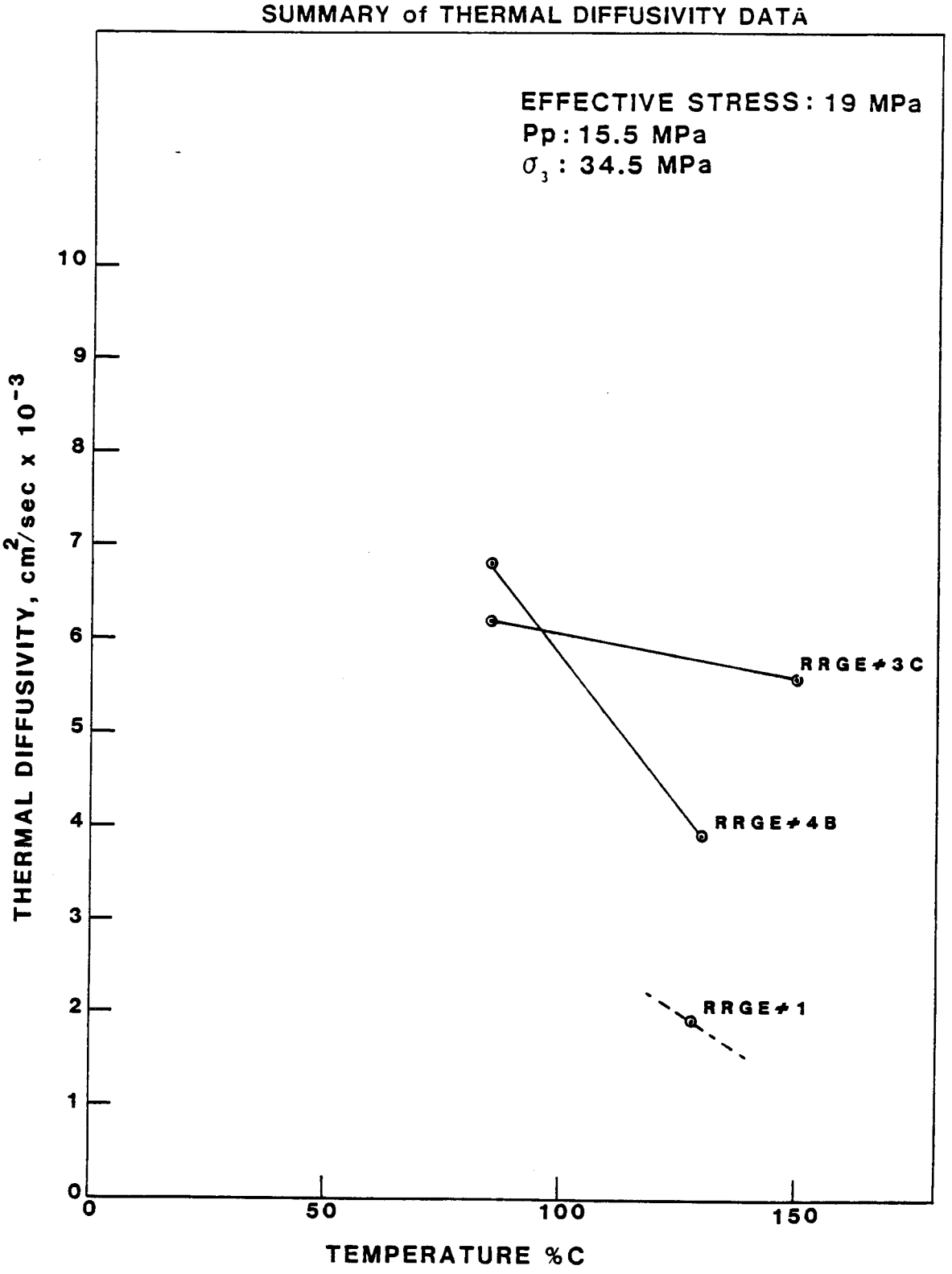

Figure 15: Summary of Thermal Diffusivity vs. Temperature for Raft River Samples.

THERMAL EXPANSION TESTS

Thermal strain (expansion) was measured as a function of temperature for test specimens from each of the four Raft River wells, RRGE #1, #2, #3C and #4B. Measurements were performed at simulated in situ stress and pore fluid pressures and at temperatures ranging from 30°C to 180°C.

Test Procedures

Sample Preparation

Core materials for testing were prepared as right circular cylinders 5.08 cm (2.00 inches) in length and 2.54 cm (1.00 inch) in diameter. Sample ends were ground flat and parallel to ±0.013 cm (±0.005 inches). Hardened steel endcaps were placed at each end and the assembly was jacketed with teflon tubing to isolate the sample from the confining fluid. Strain measuring devices were positioned on the endcaps to measure axial strains and thermocouples were located on the sample surface to measure temperature.

Prepared samples were placed in a pressure vessel, saturated with synthetic brine by vacuuming and flooding, and allowed to come to equilibrium with pressure and temperature. Generally, pore pressure reached a constant equilibrium value throughout the sample after a period of two hours at in situ conditions. During the tests, confining pressures and pore fluid pressures were maintained at 34.5 MPa (5000 psi) and 14.5 MPa (2250 psi) respectively. Temperatures were varied from 30°C (86°F) to 180°C (356°F), in preprogrammed heating and cooling cycles, at a rate less than 1°C per minute while data for sample temperature and axial strain were recorded. The thermal expansion coefficient was calculated from the slope of axial strain versus temperature curve and is accurate to ±5 percent.

Thermal Expansion Test Results

Table 6 is a summary of test results and Figures 16 through 19 show the axial strain versus temperature of a sample from each of the four Raft River wells. The sample depths range from 1280 m (4200 ft) to 1524 m (5000 ft). The strain data shown is an average value for increasing and decreasing temperatures. Noted on each plot is a value of thermal expansion determined at 150°C (the in situ reservoir temperature). This value, $\alpha_{150°C}$, is included as an estimate of the reservoir response, and was calculated from data taken between 125°C and 175°C.

Discussion and Conclusions

Thermal expansion is seen to be an essentially linear function of temperature between 30°C and 180°C. At 1288 m (4226 ft) (Well RRGE #2, Sample #211) and 1520 m (4982 ft) (Well RRGE #3C, Sample #311), the rock, a graywacke, has a coefficient of thermal expansion of approximately 7.7 x10^{-6}/°C. At 1370 m (4501 ft) (Well RRGE #1, Sample #111) and 1414 m (4640 ft) (Well RRGE #4B, Sample #411), the rock, devitrified tuff, has a coefficient of thermal expansion of approximately 11.1 x10^{-6}/°C. Reported values of thermal expansion are representative of the tested rock types, but because of the wide range of lithologies in the Salt Lake Formation, a larger sample population would be required to accurately define overall thermal response of the reservoir.

Table 6

Summary of Thermal Expansion Test Results

Confining Stress = 34.5 MPa
Pore Fluid Pressure = 15.5 MPa

Well No.*	Sample Depth (m)	Rock Type	Thermal Expansion Evaluated at 150°C (ε/°C)
RRGE #2	1288	Graywacke	7.8×10^{-6}
RRGE #1	1372	Devitrified Tuff	11.6×10^{-6}
RRGE #4B	1414	Silty Devitrified Tuff	10.6×10^{-6}
RRGE #3C	1519	Sandy Devitrified Tuff	7.6×10^{-6}

*INEL Designation

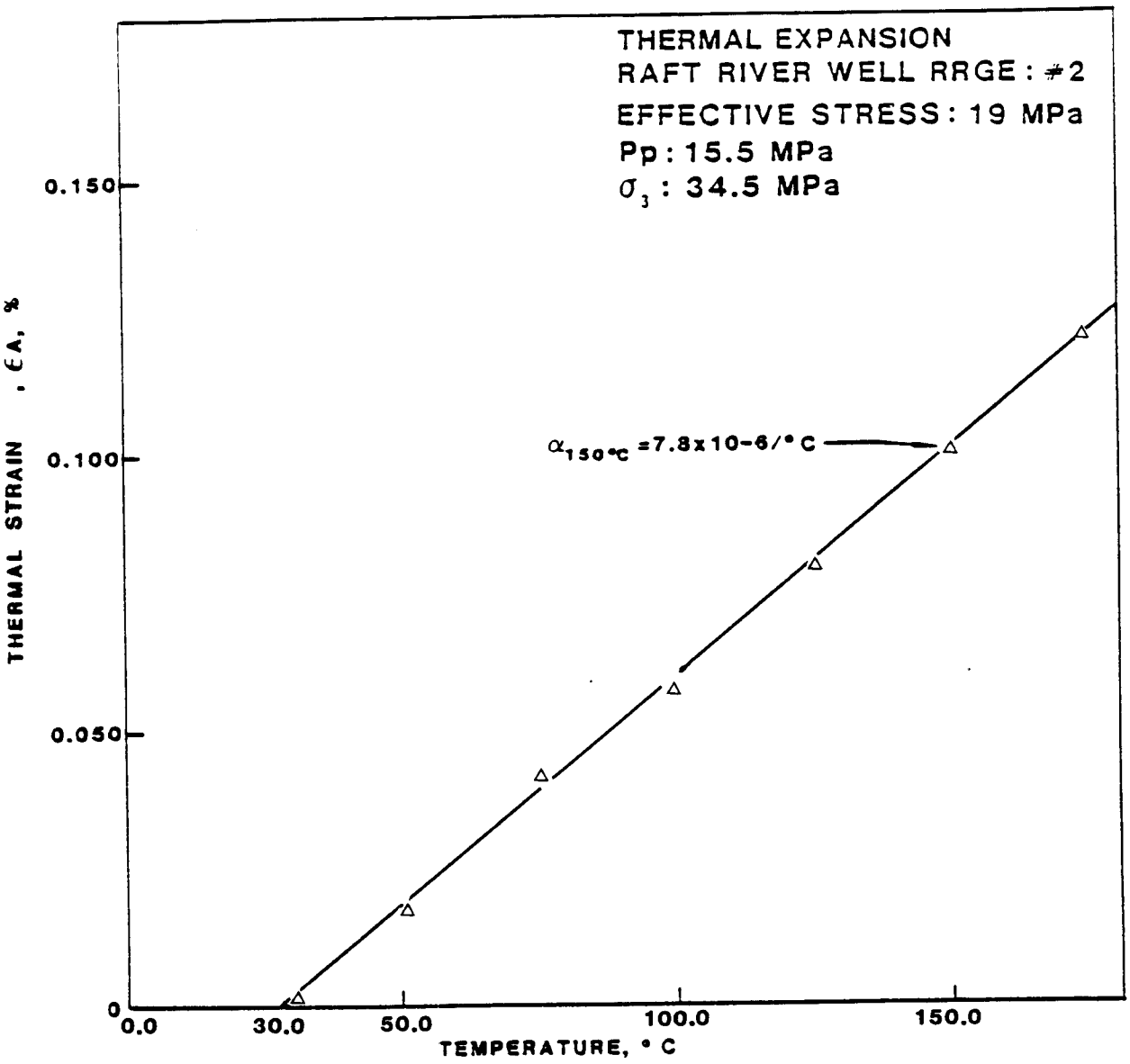

Figure 16 : Thermal Strain vs. Temperature. Raft River Well #2.

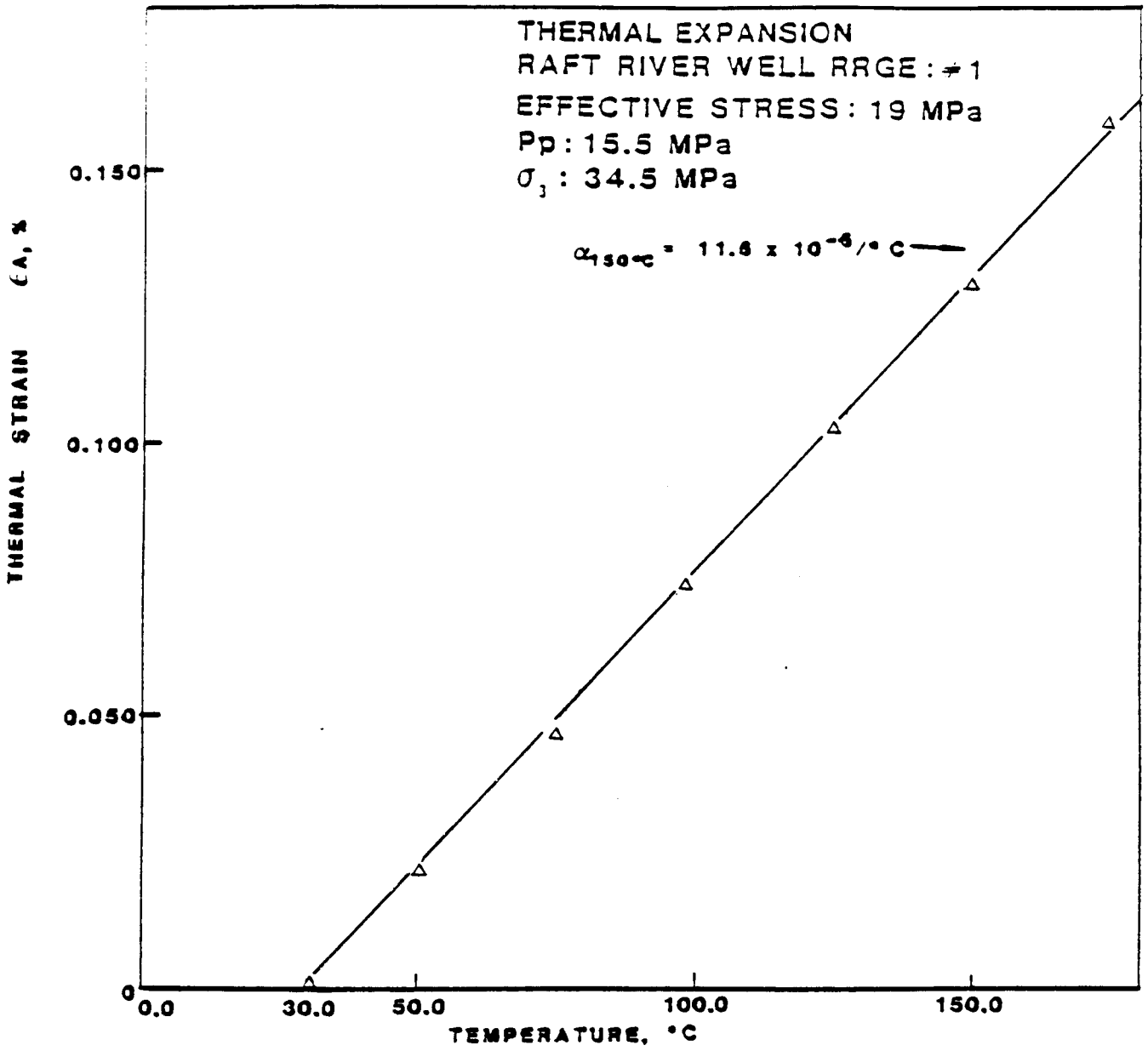

Figure 17. Thermal Strain vs. Temperature. Raft River Well #1.

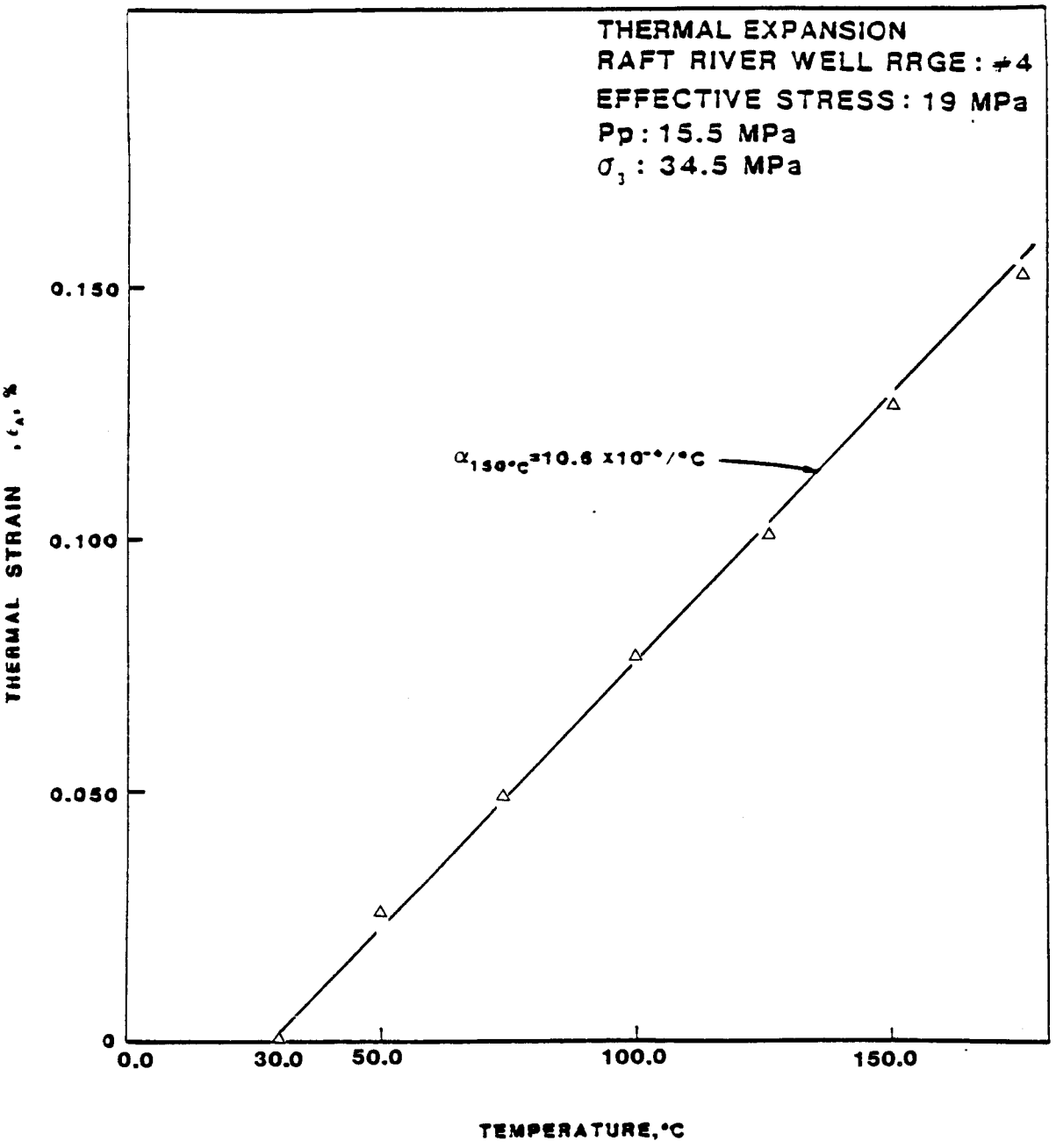

Figure 18. Thermal Strain vs. Temperature. Raft River Well #4.

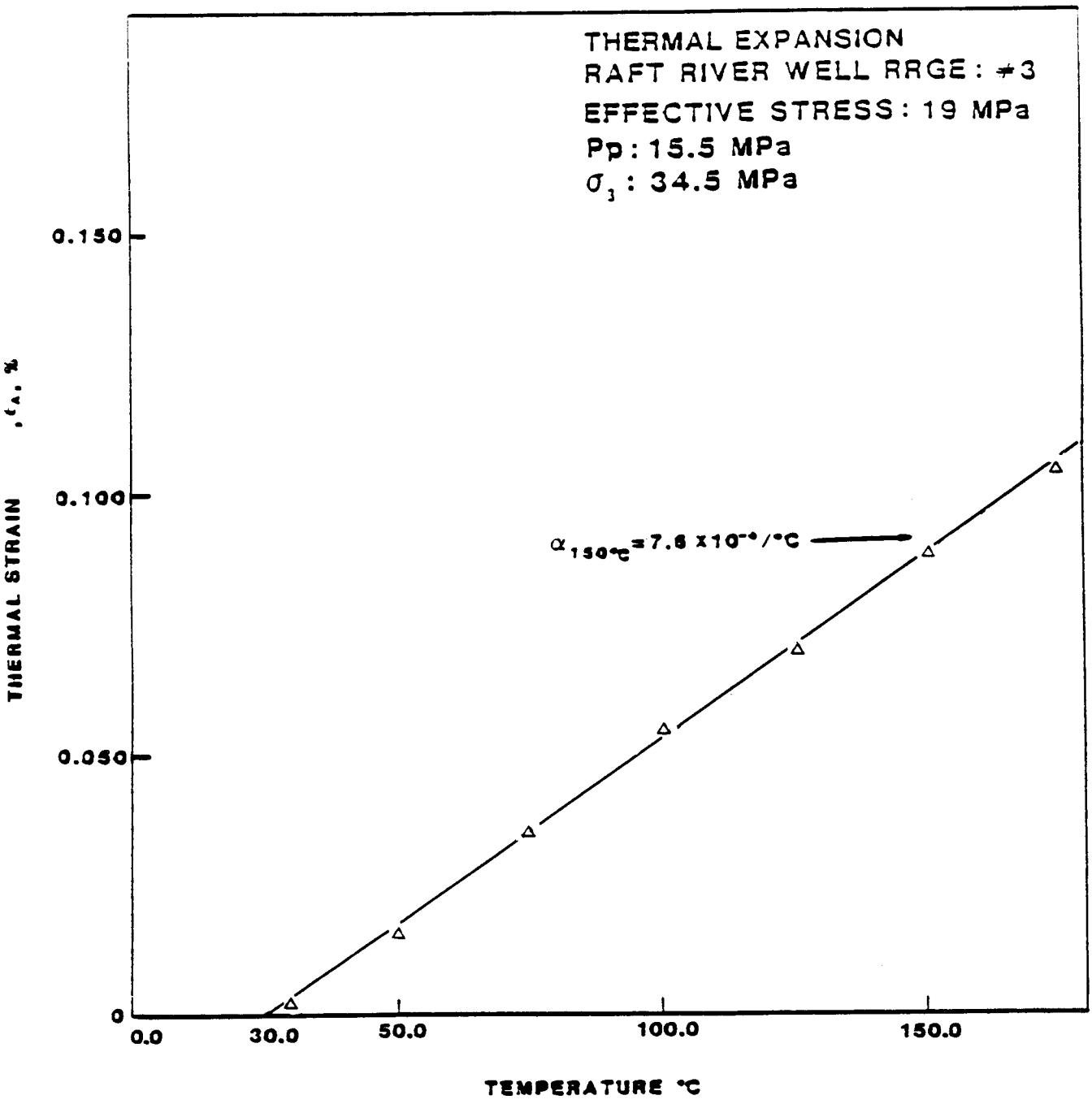

Figure 19 : Thermal Strain vs. Temperature. Raft River Well #3.

LIQUID PERMEABILITY

Permeability of one sample from each of the four Raft River wells was measured as a function of temperature. Additionally, the effect upon permeability of pore fluid flashing (phase change) at reservoir temperature was investigated. Temperature effects were determined at in situ pressure over a range of temperatures from 20°C to 150°C. The effects of pore fluid phase change were evaluated at 150°C by lowering the pore fluid pressure from the in situ value of 15.5 MPa to a value of 1.38 MPa.

Test Procedures

Sample Preparation

Samples were cored parallel to the axis of the wellbore and machined to right circular cylinders 5.08 cm (2.0 inches) in length and 5.08 cm (2.0 inches) in diameter.

Each sample was placed between two stainless steel end caps and ceramic insulators as shown in Figure 20. Diffusion disks were used to distribute the permeating brine over the ends of the sample. The sample and end caps were enclosed with two layers of silicone rubber and heat shrink teflon tubing to prevent contact between the test sample and confining fluid.

Experimental Procedure

Prepared samples were placed in a pressure vessel and allowed to come to equilibrium with temperature, pore fluid pressure and confining pressure before initiating flow through the sample. Fluid flow was achieved by the application of as much as 1.03 MPa (150 psi) differential pressure across sample ends. After flow was established at 23°C, permeability was measured at several points as the temperature was increased to 150°C. Once at in situ

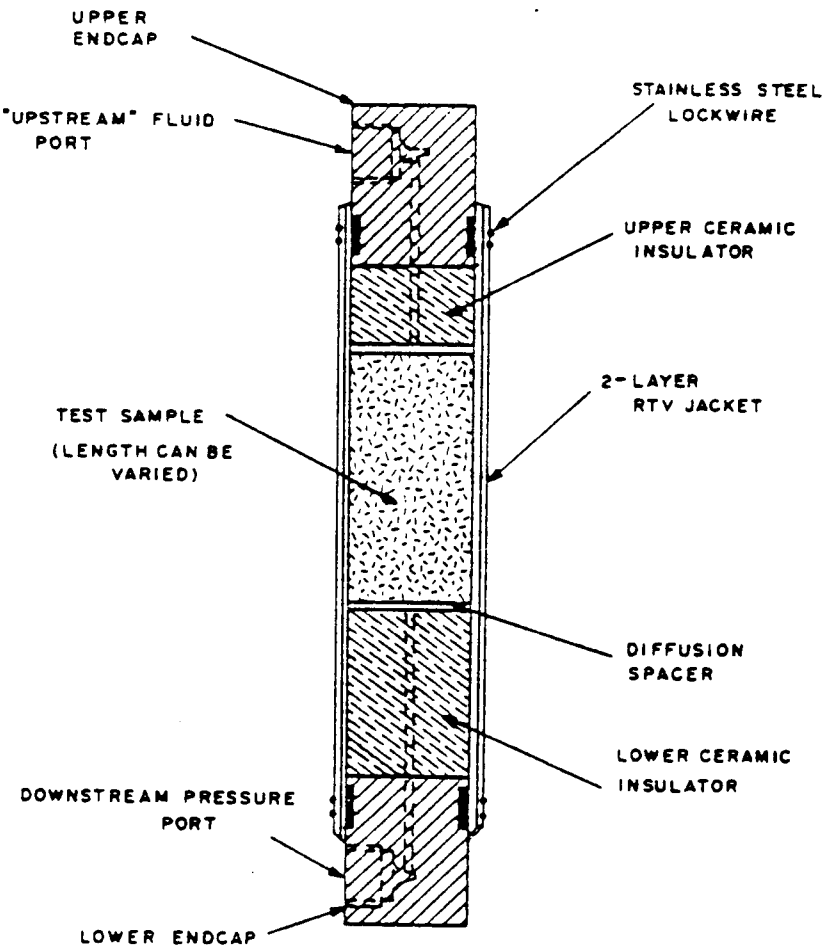

Figure 20. Permeability Sample Configuration for Raft River Core.

reservoir temperature (150°C), permeability was measured and the pore fluid pressure was lowered to 1.38 MPa (200 psi), allowing the fluid to flash. This lower pressure was maintained for 30 minutes and permeability was again measured. Pore fluid pressure was increased to its original in situ value and post-flash permeability was measured.

Liquid Permeability Test Results

Table 7 and Figure 21 are a compilation of permeability test data for Raft River core samples from Wells RRGE #1, #2, #3C and #4B. Vertical permeability (y-axis) is plotted on a 4 cycle log scale and temperature (x-axis) is plotted on a linear scale. Figures 22 through 25 show the individual perme-

Table 7

Summary of Results of Permeability Tests
Raft River Wells 1, 2, 3C and 4B

Confining Stress = 5000 psi
Pore Fluid Pressure = 2300 psi

Well Number INEL* Designation	Sample Depth (m)	Rock Type	Test Temperature (°C)	Permeability (darcy)
RRGE #2	1286	Graywacke	22	5.6×10^{-4}
			70	4.2×10^{-4}
			110	4.7×10^{-4}
			150	4.1×10^{-4}
RRGE #1	1372	Devitrified Tuff	22	3.3×10^{-4}
			70	2.8×10^{-4}
			110	2.7×10^{-4}
			150	2.5×10^{-4}
RRGE #4B	1416	Silty Devitrified Tuff	22	7.6×10^{-7}
			70	4.3×10^{-7}
			110	5.2×10^{-7}
			150	5.0×10^{-7}
RRGE #3C	1519	Sandy Devitrified Tuff	22	1.6×10^{-6}
			70	1.1×10^{-6}
			110	1.1×10^{-6}
			150	1.3×10^{-6}

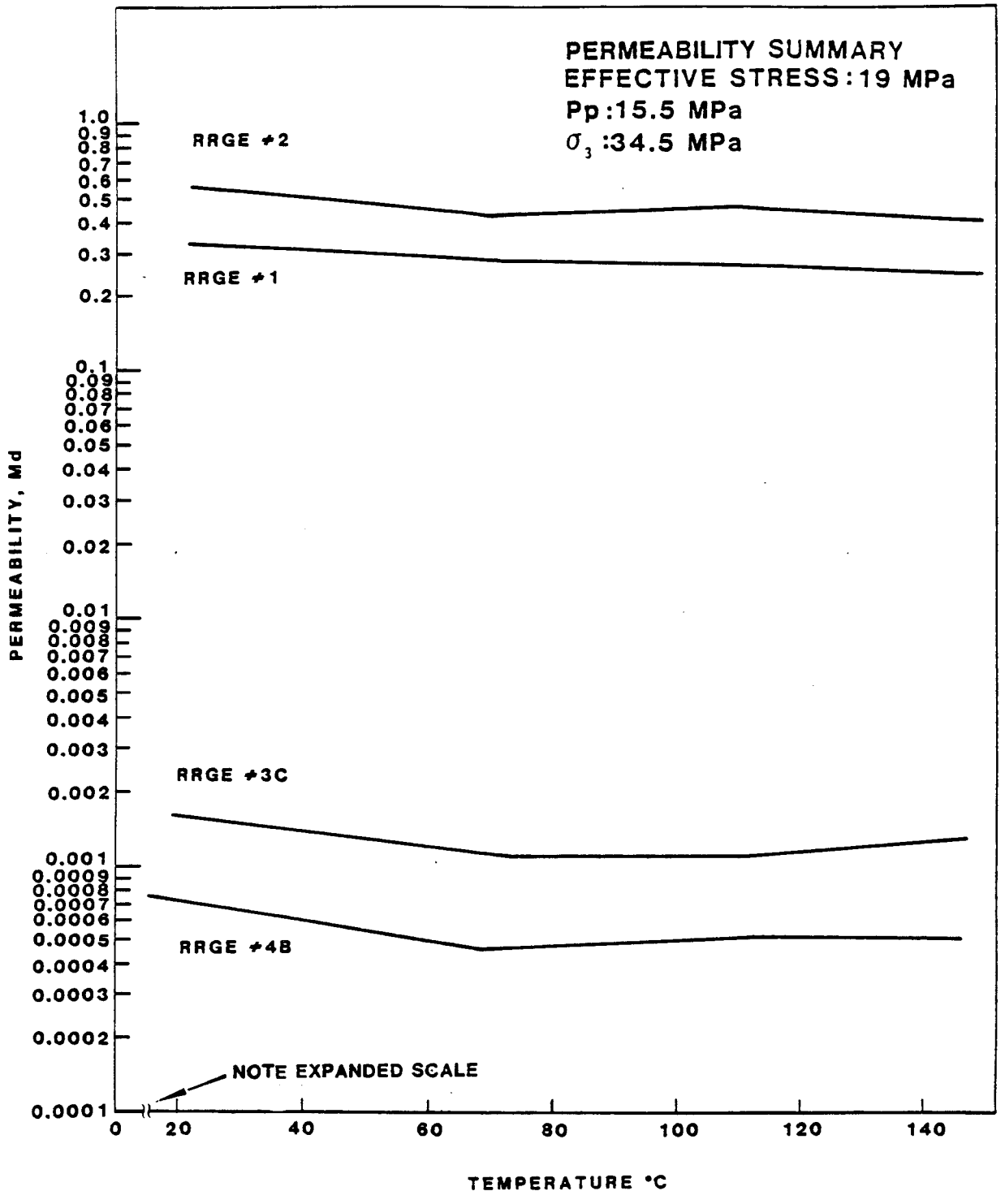

Figure 21: A summary of Permeability vs. Temperature. Raft River.

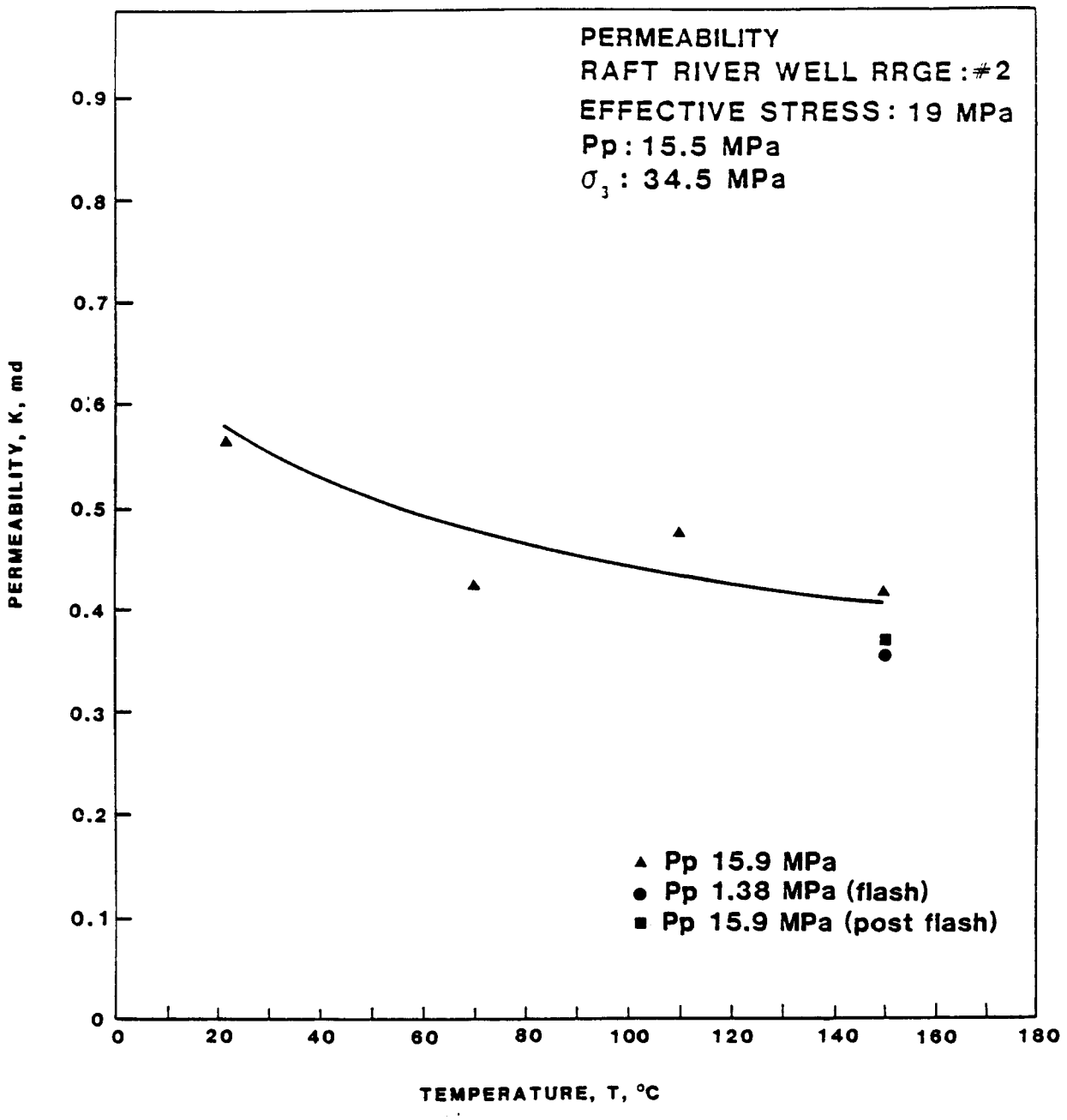

Figure 22: Permeability vs. Temperature. Raft River Well #2.

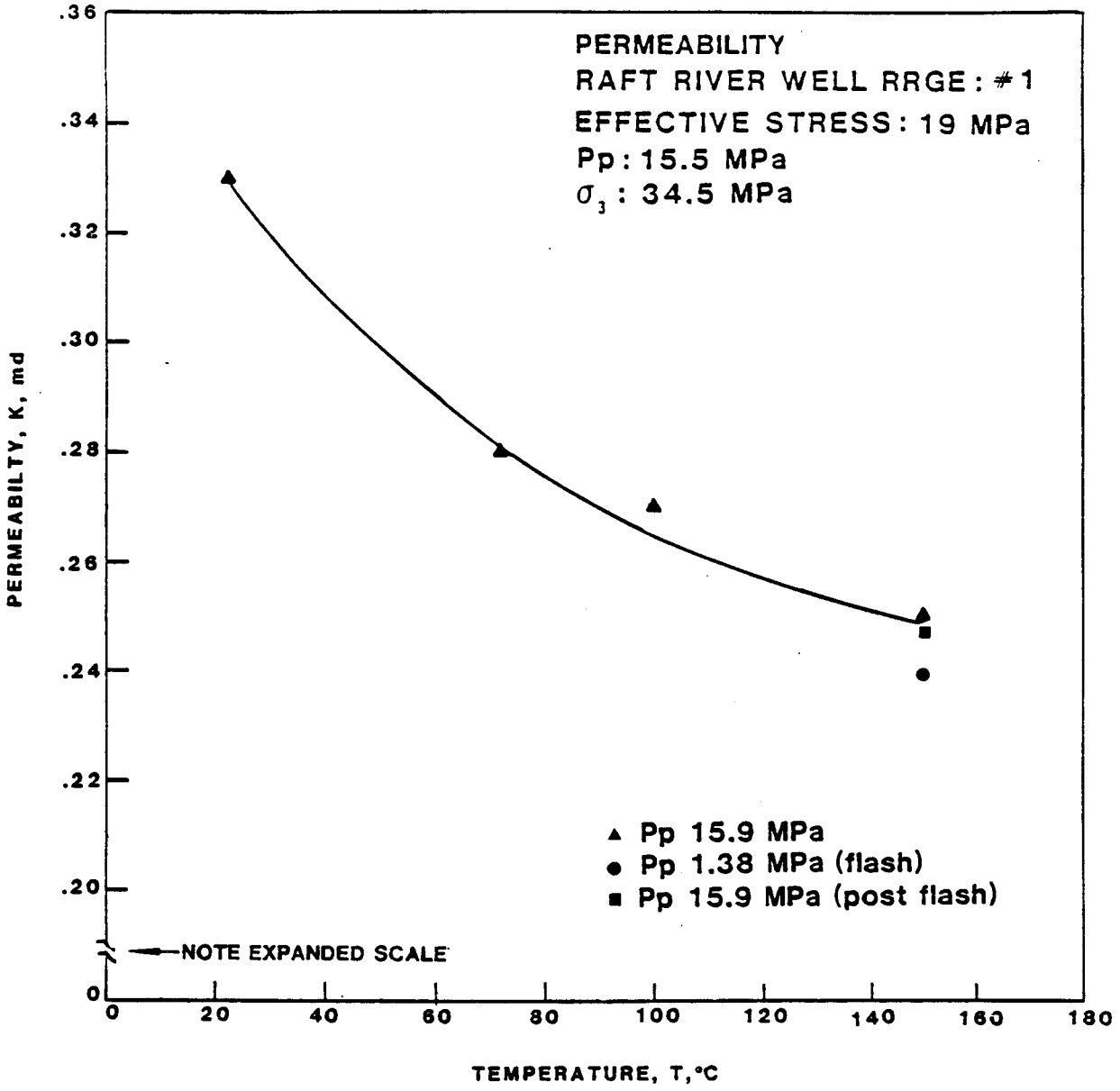

Figure 23: Permeability vs. Temperature, Raft River Well #1.

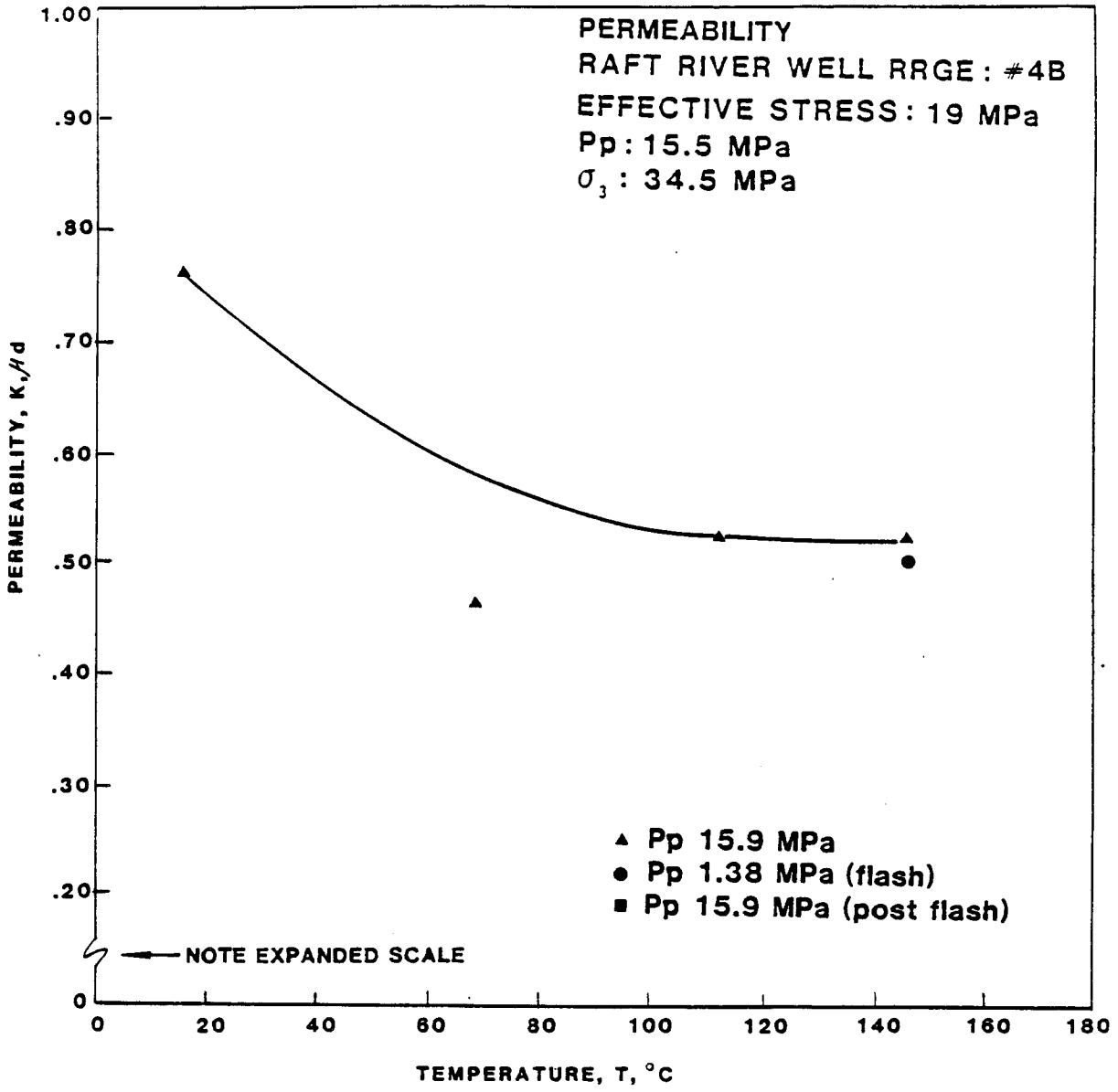

Figure 24: Permeability vs. Temperature. Raft River Well #4B.

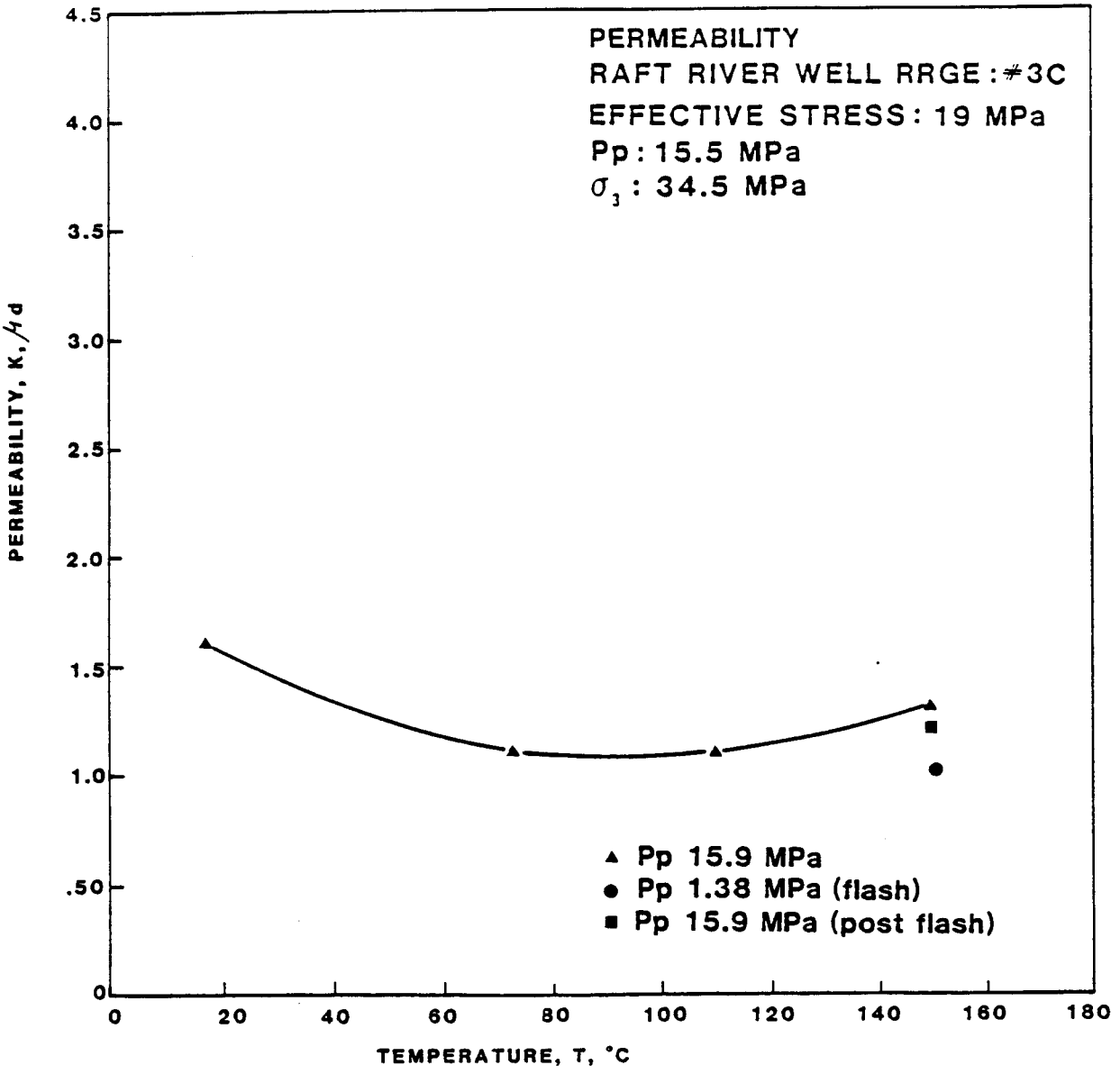

Figure 25: Permeability vs. Temperature. Raft River Well #3C.

ability test data and are plotted on conventional, linear scales. Data for flash and post-flash permeability are included.

Discussion and Conclusions

The core samples from RRGE #1 and RRGE #2 at 1372 m (4500.6 ft) and 1286 m (4219.0 ft) respectively, are over 100 times more permeable than samples from Wells RRGE #3C and RRGE #4B at 1519 m (4983.5 ft) and 1416 (4645.0 ft), respectively. Permeabilities of the samples from 1286 m (4219 ft) and 1372 m (4500 ft) ranged from 0.58 to 0.33 md and from 0.33 to 0.24 md, respectively over temperatures of 23 to 150°C. Permeabilities of the samples from 1416 m (4645 ft) and 1519 m (4983 ft) ranged from 0.76 to 0.50 $x10^{-3}$ md and from 1.60 to 1.00 $x10^{-3}$ md, respectively over temperatures of 20 to 150°C. Although the permeability values of the more shallow samples (1286 m and 1372 m) are larger by two orders of magnitude than those of the deeper samples (1416 m and 1519 m), the percent decrease in permeability at higher temperatures is similar in all samples.

Possible explanations for this difference in permeability are the difference in lithology of each core sample and differences in sample porosity with depth. The microdarcy rocks from 1420 m and 1520 m are silty and sandy devitrified tuffs with a large clay percentage, where in contrast, the millidarcy rocks, from 1290 m and 1370 m, have a considerably smaller percentage of fine textured material. Average porosity in samples from the upper zone is 21.4%, and that of samples from the lower zone is 19.2%. Because lithology and porosity profoundly affect fluid transport properties, it is reasonable to conclude that the abundance of silt and clay, together with porosity differences are the cause of the lower permeability of these samples.

Small reductions in permeability were measured as a result of pore fluid flash (phase change) conditions. Permeability decreased as much as 25% to as

little as 4% after the pore fluid flashed to the gas phase. This decrease in permeability was probably the result of larger effective stress acting upon the specimen when pore fluid pressure was lowered to cause fluid phase change.

Permeability partially recovered after returning the pore fluid to the liquid phase, final permeability impairment ranged from 1 to 9%. This small permanent decrease in permeability was probably the result of movement of the specimen's internal fines or irreversible matrix deformation resulting from the phase change pressure cycle.

ULTRASONIC VELOCITY

Ultrasonic velocity of one core sample from each of the four Raft River wells, RRGE #1, #2, #3C and #4B, was measured as a function of temperature. P-wave and S-wave velocities were determined at in situ stresses and pore fluid pressures over a range of temperatures from 20°C to 150°C. The effect of pore fluid phase change at 150°C was investigated in two of the samples. Additionally, bench condition velocities were measured in all four samples.

Dynamic moduli and Poisson's ratio of the samples were calculated from the ultrasonic velocity data.

Test Procedures

Sample Preparation

Core materials for testing were prepared as right circular cylinders, 5.08 cm (2.00 inches) in length and 5.08 cm (2.00 inches) in diameter. Sample ends were ground flat and parallel to ±0.013 cm (±0.005 inches). Endcaps, containing ultrasonic transducers were placed at each end and the assembly was jacketed with teflon tubing to isolate the sample from the confining fluid.

Experimental Procedure

Prepared samples were placed in a pressure vessel, saturated with synthetic brine by vacuuming and flooding, and allowed to come to equilibrium with temperature and pore fluid pressure. Equilibrium was assumed to exist when pore fluid pressure became invarient with time.

Ultrasonic velocities were measured using the "Through Transmission System" shown in block diagram form in Figure 26. This is an adaptation of the technique introduced by Mattaboni and Schreiber, and is capable of mea-

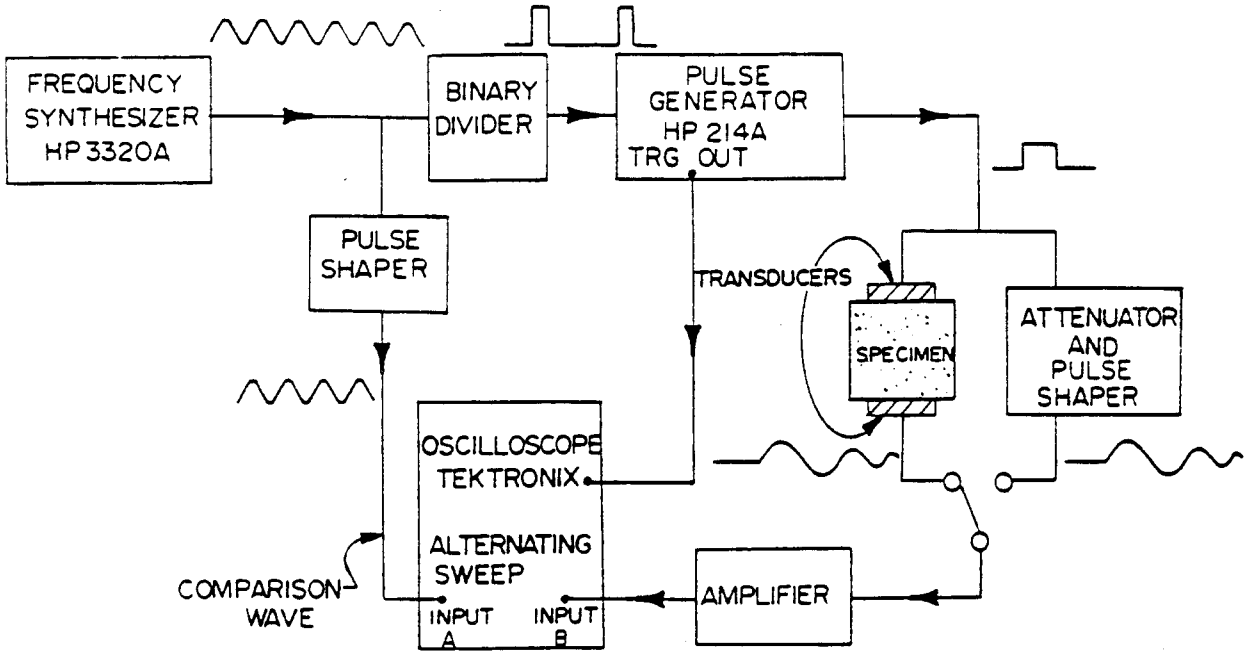

Figure 26. Through-Transmission System

suring small elapsed times to a high degree of accuracy. Time measurement is derived from the frequency of a very stable frequency synthesizer (stability ±1 part in 10^7/month, accuracy ±0.001 percent).

The signal passing through the specimen was viewed on an oscilloscope and compared with the signal from the variable frequency synthesizer (comparison wave). The latter was modified by a pulse shaper to exactly match the wave which has passed through the specimen. Next, the pulse which excited the transmitting transducer was viewed, and its shape matched to that of the comparison wave. Once the pulse shapes were matched, they were made to coincide on the oscilloscope to a high degree of precision. The frequency of the synthesizer was then adjusted for an exact number of cycles between the transmitted signal and the signal through the specimen. The transit time of the ultrasonic wave through the material was obtained by dividing the number of

cycles by the frequency. The velocity of the acoustic wave in the specimen was obtained by dividing the path length by the corrected elapsed time.

The overall accuracy of this technique is limited mainly by the accuracy with which the wave forms can be matched on the oscilloscope, the resulting average accuracy is ±1.5%.

Ultrasonic Velocity Test Results

Figure 27 is a compilation of P and S wave velocity data plotted as a function of temperature. Table 8 is a summary of test results and of dynamic moduli calculated from ultrasonic velocity data obtained at *in situ* temperature, stress and pore fluid pressure. Figures 28 through 31 show P and S wave data at bench conditions as well as at reservoir pressure with temperature ranging from 25°C to 150°C. Additionally shown on plots 28 through 31 are velocity data for pore fluid flash and post-flash conditions at 150°C.

Discussion and Conclusions

As shown in Figure 27, ultrasonic velocity decreases slightly with increasing temperature. At 23°C P-wave velocities ranged from 3.6 to 4.7 km/sec and S-wave velocities ranged from 2.2 to 2.7 km/sec. At 150°C P-wave velocities decreased by 1 to 5% and S-wave velocities decreased by 2 to 7%. The changes in velocity were fairly uniform functions of temperature for each sample, but do not correlate with sample depth.

The phenomenon of decreasing velocity with increasing temperature is probably a result of the opening of microcracks in the rock which thereby slow transmission velocity by increasing the wave's average path length. Under hydrostatic loading the microcracks are compressed and closed, and ultrasonic velocities are increased. As a rock sample is heated, its constituent grains expand at different rates. The grains that expand the most tend to prop open

Table 8

Summary of Ultrasonic Velocity Measurement Results

Well*	Sample Depth (m)	Rock Description	Effective Compressive Stress (MPa)	Test Temp. (°C)	P-Wave Velocity (km/s)	S-wave Velocity (km/s)	Young's Modulus (MPa)	Bulk Modulus (MPa)	Shear Modulus (MPa)	Poisson's Ratio
RRGE #2	1287	Graywacke	19	150	3.70	2.14	22,670	14,330	9,170	0.24
RRGE #1	1370	Silty Mudstone	19	150	4.05	2.31	26,200	17,170	10,500	0.25
RRGE #4B	1385	Silty Devitrified	19	150	4.70	2.38	37,200	35,700	14,000	0.33
RRGE #3C	1519	Silty Tuff & Graywacke	19	150	4.18	2.51	39,000	22,340	16,100	0.21

*INEL Designation

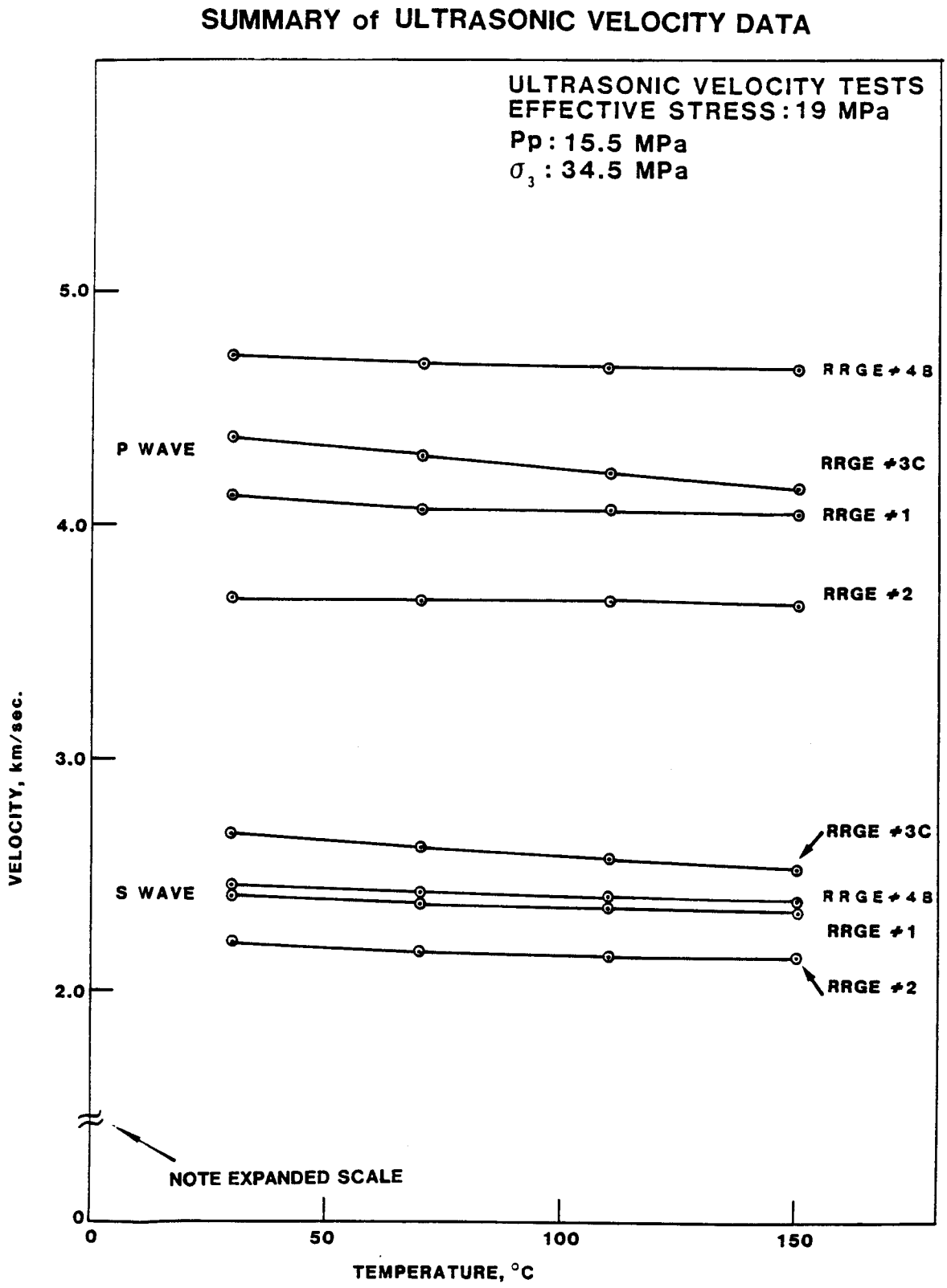

Figure 27: A summary of Ultrasonic Velocity tests performed on Raft River core.

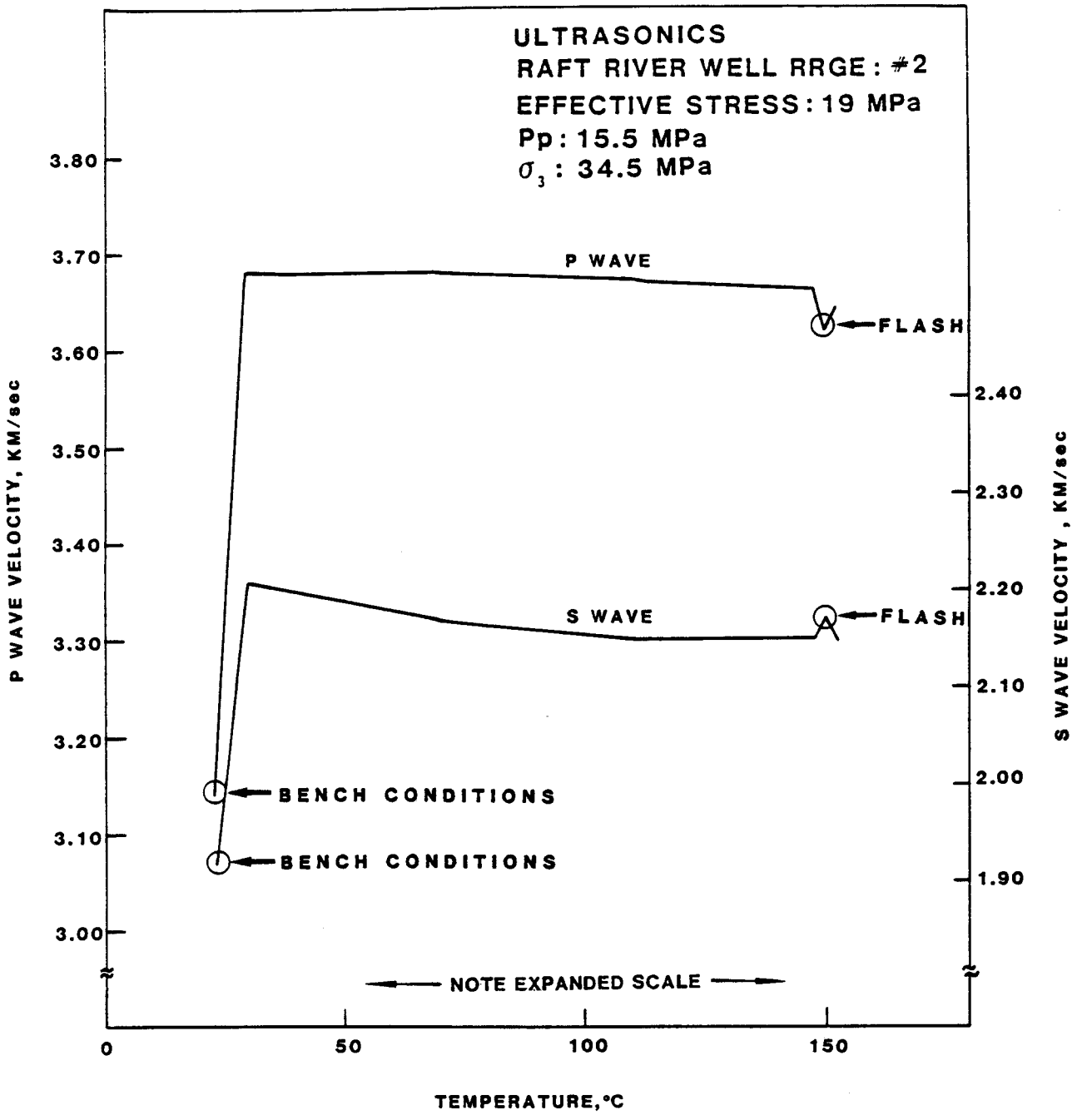

Figure 28: Ultrasonic Velocities vs. Temperature. Raft River Well #2.

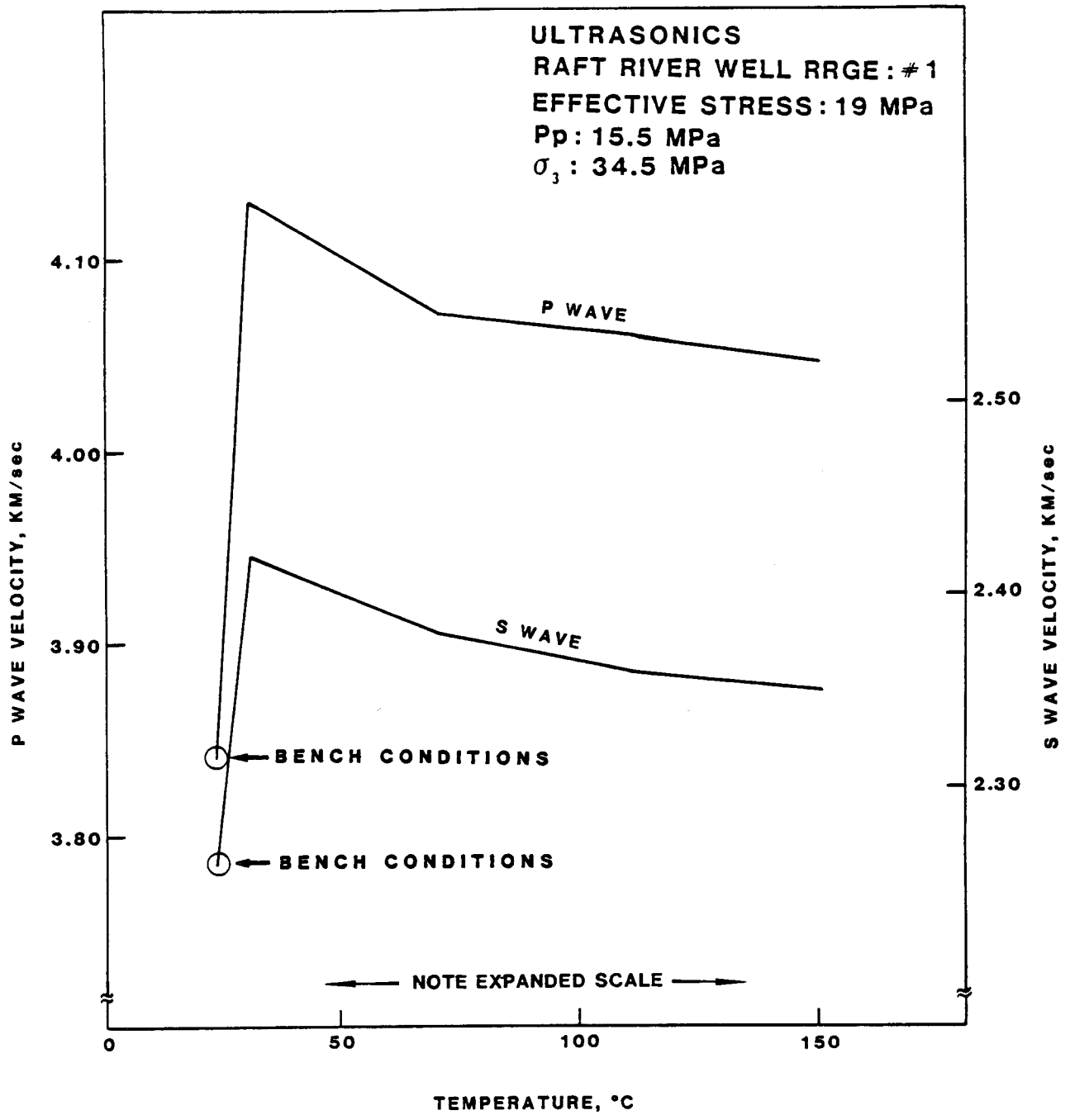

Figure 29: Ultrasonic Velocities vs. Temperature. Raft River Well #1.

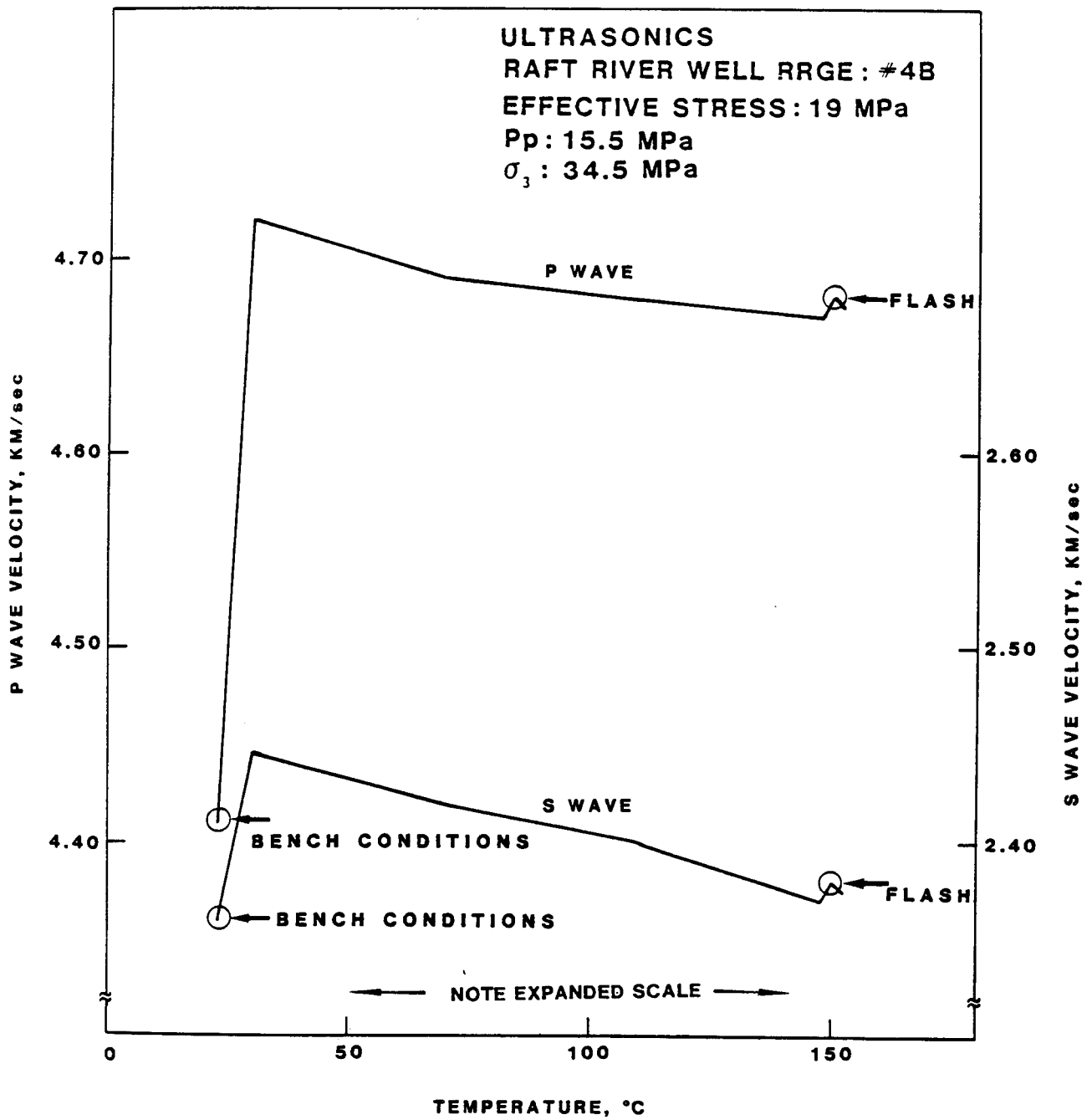

Figure 30 : Ultrasonic Velocities vs. Temperature. Raft River Well #4B.

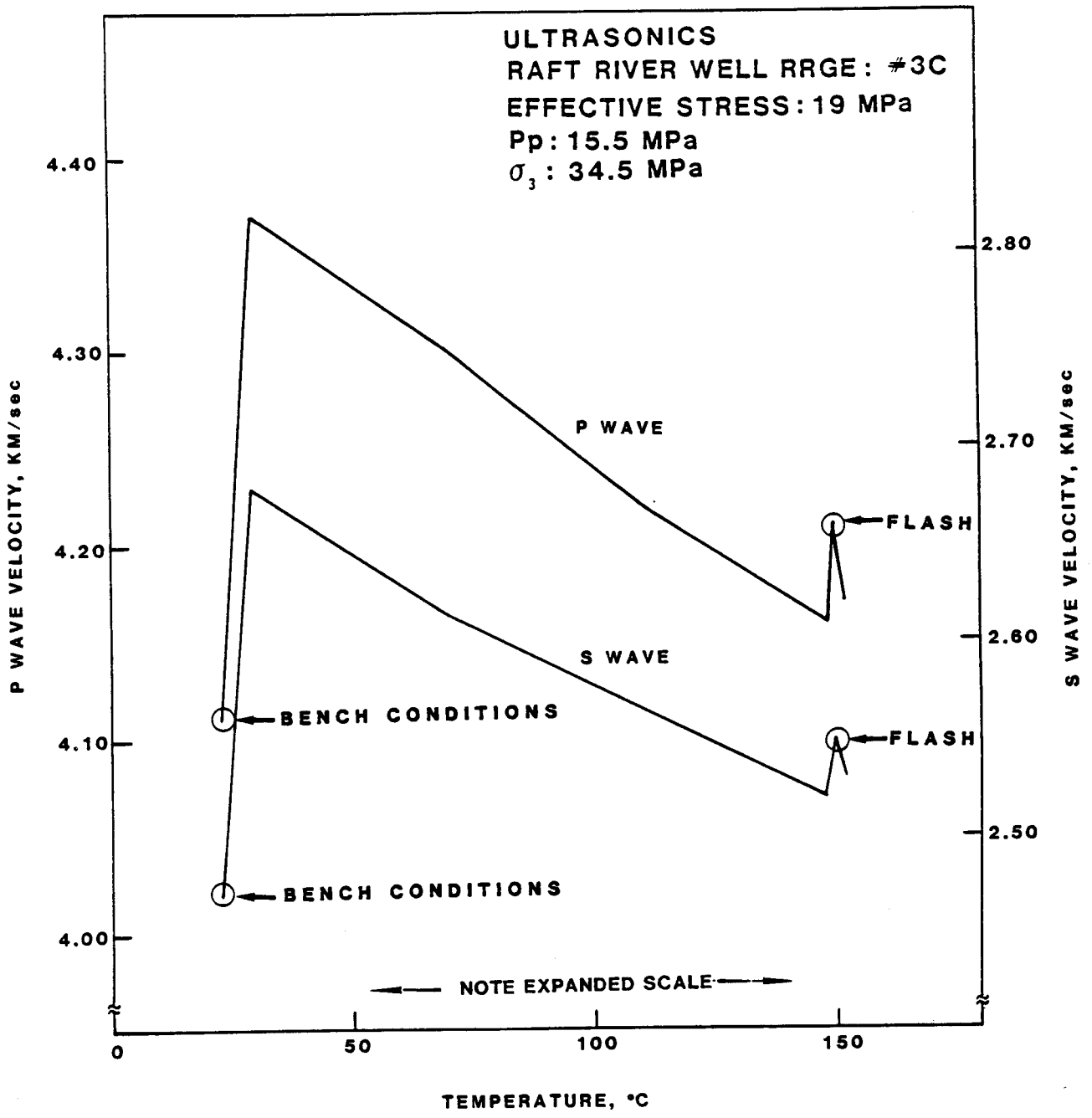

Figure 31: Ultrasonic Velocities vs. Temperature. Raft River Well #3C.

existing microcracks and decrease ultrasonic velocities. If rock constituents expand uniformly the change in ultrasonic velocity is less pronounced.

Changes in ultrasonic velocities due to flashing of pore fluid are minor. The significant results in these tests are that velocities change by only 1 to 3% during flash and return to their initial values when normal well pressures are reinstated.

Comparisons between Poisson's ratio and Young's modulus values derived from ultrasonics vs. triaxial tests show that when calculated from ultrasonics data, Poisson's ratio is approximately 50% higher, and Young's modulus is approximately 100% higher. These results are not uncommon in that static values of Young's modulus are sensitive to mechanically compliant cracks, whereas acoustic waves tend to bypass these cracks. Comparisons of individual test results may vary considerably from this, but the general trend is evident.

REFERENCES

1. Carslaw, H.S. and Jaeger, J.C., "Conduction of Heat in Solids," Clarendon Press, Oxford, England, 1959.

2. Godwin, L.H., Haigler, L.B., Rious, R.L., White, D.E., Muffler, L.J.P., and Wayland, R.G., 1971, "Classification of Public Lands Valuable for Geothermal Steam and Associated Geothermal Resources," U.S. Geological Survey Circular 647," 17 p.

3. Keys, W.S. and Sullivan, J.K., "Role of Borehole Geophysics in Defining the Physical Characteristics of the Raft River Geothermal Reservoir, Idaho," Geophysics, Vol. 44, pp. 1116-1141, 1979.

4. Kolesar, P., Written Communication, 1979 in "Subsurface Geology of the Raft River Geothermal Area, Idaho," by H.R. Covington, GRC, Transactions, Vol. 4, 1980.

5. Mabey, D.R., Hoover, D.B., O'Donnel, J.E. and Wilson, C.W., "Reconnaissance Geophysical Studies of the Geothermal System in Southern Raft River Valley, Idaho," Geophysics, Vol. 43, pp. 1470-1484, 1978.

6. Mattaboni, P., Schreiber, E., "Methods of Pulse Transmission Measurements for Determining Sound Velocities," Journal of Geophysical Research, Vol. 70, NO. 20, pp. 5160-5163, 1967.

7. Urban, T.C. and Diment, W.H., 1975, "Heat Flow on the South Flank of the Snake River Rift," Geol. Soc. America Abstract with Programs, V. 7, No. 5, p. 648.

8. Williams, P.L., Mabey, D.R., Zohdy, A.A.R., Ackermann, H., Hoover, D.B., Pierce, K.L. and Oriel, S.S., 1976, "Geology and Geophysics of the Southern Raft River Valley Geothermal Area, Idaho, USA, 1976," Second United Nations Symposium on the Development and Use of Geothermal Resources, San Francisco, Calif., May 20-29, 1975, V. 2, p. 1273-1282.

9. Woodside, W. and Messmer, J.H., "Thermal Conductivity of Porous Media: I. Unconsolidated Sands," Journal of Applied Physics, Vol. 32, No. 9, Sept., 1961, pp. 1688-1698.

APPENDIX

TRANSIENT THERMAL CONDUCTIVITY MEASUREMENT TECHNIQUE

Theory

The equation governing the temperature, θ, at a point in an infinite mass containing a uniform linear heat source can be determined as[1]:

$$\theta(r, t) = \frac{P}{2\pi K} \; I \; \frac{r}{2(\alpha t)^{1/2}} \qquad (1)$$

where P = power input per unit length of heat source (W/m)

K = thermal conductivity of the mass (W/m-K)

α = thermal diffusivity of the mass (m-m/s)

r = radial distance from source (m)

t = time from start of energy input (s)

and I is the function

$$I(x) = C \;\; \ln x + \frac{x^2}{2} - \frac{x^4}{8} + \ldots \qquad (2)$$

where C is Euler's constant, 0.5772.

Considering the case where the radial distance becomes very small ($r \to 0$) the term, $x = [r/2(\alpha t)^{1/2}]$, also becomes very small. Assuming that this situation occurs in the experimental set-up, the terms in the expansion of I(x) of order x^2 and higher can be regarded as negligible. This assumption appears to be good for the present experimental system where the thermocouple is attached directly to the heater.

Therefore,

$$\theta(r, t) = \frac{P}{2\pi K} \; C - \ln \; \frac{r}{2(\alpha t)^{1/2}} \qquad (3)$$

---

[1]Woodside, W. and Messmer, J.H., 1961, Thermal conductivity of porous media: I. Unconsolidated sands: J. Applied Physics, V. 32, n. 9, p. 1688-1698.

Temperature rise, $\Delta\theta$, between times t_1 and t_2 can then be described:

$$\Delta\theta = \theta(r, t_2) - \theta(r, t_1) \tag{4}$$

This expression with some algebraic manipulation gives:

$$\Delta\theta = \frac{P}{4\pi K} \ln \frac{t_2}{t_1} \tag{5}$$

From Equation (5) it can be seen that the term ($P/4\pi K$) represents the slope of θ versus ln(t) curve. With carefully monitored voltages and current applied to the linear heat source, the power dissipated per unit length, P, can be determined allowing the calculation of the thermal conductivity.[2]

Several major sources of error are possible in this method. The first is due to the elimination of the higher order terms of the I(x) function. Direct attachment of the thermocouple eliminates this error. Secondly, the contact resistance of the probe to the sample can influence the time-temperature curve. This error is eliminated by the use of a standardized, highly conductive potting compound and disregarding the initial portion of the curve. Finally the power input to the probe can vary due to the resistance change of the probe with temperature. This effect can be minimized by the use of a constant current power supply and careful monitoring of the probe voltage. Probes showing voltage variation greater than 1 percent are not used.

---

[2]Carslaw, H.S. and Jaeger, J.C., "Conduction of Heat in Solids," Clarendon Press, Oxford, England, 1959.

THERMAL DIFFUSIVITY MEASUREMENT TECHNIQUE

Thermal diffusivity can be evaluated from classical theory of radial heat flow in a cylinder with zero initial temperature and surface temperature $\phi(t)$. For times $t > 0$ the temperature at any point in that cylinder can be expressed

$$\theta(r, t) = \frac{2\kappa}{r_o} \sum_{n=1}^{\infty} e^{-\kappa\delta_n^2 t} \frac{\delta_n J_0(r\delta_n)}{J_1(r_o\delta_n)} \int_0^t e^{\kappa\delta_n^2 t} \phi(\lambda)d\lambda \qquad (1)$$

where θ = temperature at an arbitrary point in the sample (°C)

$\phi(t)$ = temperature at the sample surface

r_o = outer radius (meters)

r = radius (meters)

t = time (seconds)

$J_0(x), J_1(x)$ = Bessel functions

δ_n = positive roots of $J(ax_n) = 0$, $n = 1,2,\ldots$, where a is a constant

κ = thermal diffusivity (meter-meter/second)

If the surface temperature is oscillated, i.e. $\phi(t) = V \sin(\omega t)$, then the integral in Equation (1) can be computed to yield the temperature at any point in the cylinder as a function of r and t.

$$\theta(r, t) = \frac{V M_o(\omega' r)}{M_o(\omega' r_o)} \sin [\omega t + \theta_o(\omega' r) - \theta_o(\omega r_o)] + 2 \frac{\kappa V}{r_o} \sum_{n=1}^{\infty} e^{-\kappa\delta_n^2 t} \frac{\delta_n \omega J_0(r\delta_n)}{(\kappa^2 \delta_n^4 + \omega^2) J_1(r_o\delta_n)} \qquad (2)$$

where V = amplitude of the sinusoidal oscillation (°C)

ω = angular frequency

$\omega' = (\omega/\kappa)^{\frac{1}{2}}$

and

$M_o(z)e^{i\theta_o(z)} = \text{ber } z + i \text{ bei}(z) = J(ze^{3/4 \pi i})$

In sufficiently long time, $e^{-\kappa\delta n^t}$ approaches zero and the transient portion of Equation 2 vanishes. Mathematically:

$$\frac{2\kappa V}{r_o} \sum_{n=1}^{\infty} e^{-\kappa\delta_n t} \frac{\delta_n \omega J_o(r\delta_n)}{(\kappa^2\delta_n^4 + \omega^2)\, J\,(r_o\delta_n)} \quad \underset{t \to \infty}{} \quad 0$$

$$\theta(r, t) = \frac{V\, M_o(\omega' r)}{M_o(\omega' r_o)} \sin\left[\omega t + \theta_o(\omega' r) - \theta_o(\omega' r_o)\right] \tag{3}$$

If the temperature is measured at r = 0 then

$$\theta(o, t) = \frac{V}{M_o(\omega' r_o)} \sin\left[\omega t - \theta_o(\omega' r_o)\right]$$

Since the steady-state solution is a function of the same angular frequency as the surface temperature and differs only in amplitude and phase (Figure A-1), then the oscillating portion of the solution can be expressed as:

$$\sin\left[\omega t - \theta_o(\omega' r_o)\right] = \sin\left[\omega(t - \Delta t_c)\right] \tag{4}$$

where t_c = time for one period of oscillation

Δt_c = time lag between a temperature at the surface of the cylinder and the temperature at the center of the cylinder

thus

$$\omega t - \theta_o(\omega' r_o) = \omega(t - \Delta t_c)$$

or

$$\theta_o(\omega' r_o) = \omega \Delta t_c \tag{5}$$

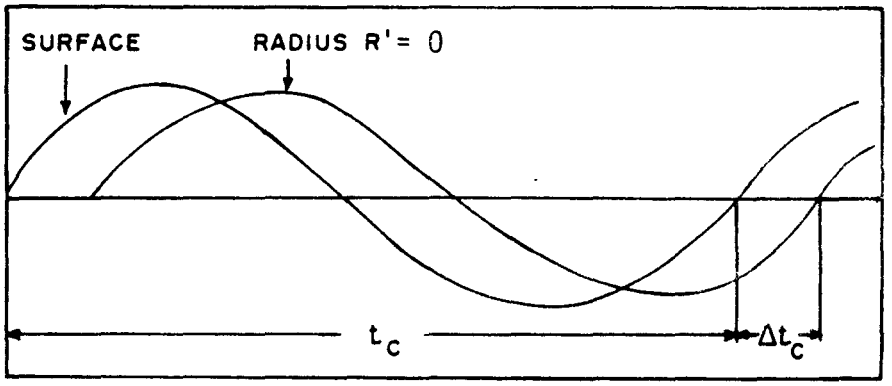

Figure A-1. Temperature Versus Time for the Surface and Center of a Cylinder.

where

$$\omega = \frac{2\pi}{t_c} \text{ and } \omega' = \left(\frac{\omega}{\kappa}\right)^{\frac{1}{2}}$$

Solving Equation 5 for thermal diffusivity, κ, we obtain

$$\kappa = \frac{r_o}{\theta_o^{-1} \frac{2\pi}{t_c} \Delta t_c}^2 \frac{2\pi}{t_c} \qquad (6)$$

where

$$\theta_o(z) = \tan^{-1} \frac{\text{bei}(z)}{\text{ber}(z)} \quad .$$

Thus by knowing the time lag Δt_c, the period of oscillation $\frac{2\pi}{t_c}$, and the sample radius r_o, the thermal diffusivity κ can be computed.

PERMEABILITY MEASUREMENT TECHNIQUE

Permeability is calculated according to the Darcy Law:

$$K = \frac{Q_r \mu L}{A \Delta P}$$

where:

K = permeability, darcies

Q_r = flow rate at reference point, ml/sec (measured at T = 23°C, constant)

μ = viscosity at flow temperature, cps (temperature dependent)

L = sample length, cm

A = cross-sectional flow area, cm^2

ΔP = pressure differential, bars (absolute)

The specific volume ratio at the front of this equation constitutes a volumetric correction for fluid volume expansion at the flow temperature since flow rate measurements are made at a reference point with constant 23°C temperature. Pressure differential is maintained constant during the course of the test. All other parameters on the right side of this equation can be physically measured from the sample or determined from published data on the properties of water at temperature and pressure.

Calculation of Moduli from Ultrasonic Velocity Values

The following relationships were used to calculate moduli from ultrasonic velocity measurements

where: V_s = Shear-wave velocity

V_p = Plane-wave velocity

ρ = Density

A. Young's Modulus, E

$$E = \frac{3\rho V_s^2 (V_p^2 - 4/3 V_s^2)}{V_p^2 - V_s^2}$$

B. Bulk Modulus, K

$$K = \rho (V_p^2 - 4/3 V_s^2)$$

C. Shear Modulus, G

$$G = \rho V_s^2$$

D. Poisson's Ratio, ν

$$\nu = \frac{E - 2G}{2G} = \frac{1/2 V_p^2 - V_s^2}{V_p^2 - V_s^2}$$